LY6E impairs coronavirus fusion and confers immune control of viral disease

Stephanie Pfaender[1,2,3#], Katrina B. Mar[4#], Eleftherios Michailidis[5], Annika Kratzel[1,2], Dagny Hirt[1,2], Philip V`kovski[1,2], Wenchun Fan[4], Nadine Ebert[1,2], Hanspeter Stalder[1,2], Hannah Kleine-Weber[6,7], Markus Hoffmann[6], H. Heinrich Hoffmann[5], Mohsan Saeed[5,8], Ronald Dijkman[1,2], Eike Steinmann[3], Mary Wight-Carter[9], Natasha W. Hanners[10], Stefan Pöhlmann[6,7], Tom Gallagher[11], Daniel Todt[3,12], Gert Zimmer[1,2], Charles M. Rice[5*], John W. Schoggins[4*], and Volker Thiel[1,2*]

[1]Institute of Virology and Immunology, Bern and Mittelhäusern, Switzerland. [2]Department of Infectious Diseases and Pathobiology, Vetsuisse Faculty, University of Bern, Bern, Switzerland. [3]Department for Molecular & Medical Virology, Ruhr-Universität Bochum, Germany. [4]Department of Microbiology, University of Texas Southwestern Medical Center, Dallas, TX, USA. [5]Laboratory of Virology and Infectious Disease, The Rockefeller University, New York, NY, USA. [6]Deutsches Primatenzentrum GmbH, Leibniz-Institut für Primatenforschung, Göttingen, Germany. [7]Faculty of Biology and Psychology, University Göttingen, Göttingen, Germany. [8]Department of Biochemistry, Boston University School of Medicine, Boston, MA, USA; National Emerging Infectious Diseases Laboratories, Boston University, Boston, MA, USA. [9]Animal Resource Center, University of Texas Southwestern Medical Center, Dallas, TX, USA. [10]Department of Pediatrics, University of Texas Southwestern Medical Center, Dallas, TX, USA [11]Department of Microbiology and Immunology, Loyola University Chicago, Chicago, USA. [12]European Virus Bioinformatics Center (EVBC), Jena, Germany

#equally contributing authors, *equal senior authorship

*e-mail: volker.thiel@vetsuisse.unibe.ch, john.schoggins@utsouthwestern.edu, ricec@rockefeller.edu

ABSTRACT

Zoonotic coronaviruses (CoVs) are significant threats to global health, as exemplified by the recent emergence of severe acute respiratory syndrome coronavirus 2 (SARS-CoV-2)[1]. Host immune responses to CoV are complex and regulated in part through antiviral interferons. However, the interferon-stimulated gene products that inhibit CoV are not well characterized[2]. Here, we show that interferon-inducible lymphocyte antigen 6 complex, locus E (LY6E) potently restricts cellular infection by multiple CoVs, including SARS-CoV, SARS-CoV-2, and Middle East respiratory syndrome coronavirus (MERS-CoV). Mechanistic studies revealed that LY6E inhibits CoV entry into cells by interfering with spike protein-mediated membrane fusion. Importantly, mice lacking Ly6e in hematopoietic cells were highly susceptible to murine CoV infection. Exacerbated viral pathogenesis in Ly6e knockout mice was accompanied by loss of hepatic and splenic immune cells and reduction in global antiviral gene pathways. Accordingly, we found that Ly6e directly protects primary B cells and dendritic cells from murine CoV infection. Our results demonstrate that LY6E is a critical antiviral immune effector that controls CoV infection and pathogenesis. These findings advance our understanding of immune-mediated control of CoV *in vitro* and *in vivo*, knowledge that could help inform strategies to combat infection by emerging CoV.

Coronaviruses (CoVs) are enveloped RNA viruses with broad host tropism and documented capability to cross the species barrier to infect humans[3]. The mammalian innate immune response controls CoV infection partly through the action of interferons (IFNs)[2,4,5]. IFNs inhibit viral infection by inducing hundreds of genes, many of which encode antiviral effectors[6]. The interferon-stimulated genes (ISGs) that inhibit CoV infection are not well defined[2]. To address this knowledge gap, we screened our published library of >350 human ISG cDNAs[7,8] in human hepatoma cells for antiviral activity against the endemic human CoV 229E (HCoV-229E) (**Extended Data Table 1, Extended Data Table 2**). The ISG lymphocyte antigen 6 complex, locus E (LY6E) strikingly inhibited HCoV-229E infection (**Fig. 1a-b**, **Extended Data Fig. 1a**). This was unexpected since we and others previously reported that LY6E enhances cellular infection by influenza A virus, flaviviruses, and HIV-1[9-11], with HIV-1 being an exception as opposing roles of LY6E have been described[12]. To verify this result, we generated stable cell lines ectopically expressing LY6E and infected cells with diverse CoVs. In addition to HCoV-229E (**Fig. 1c**), LY6E significantly inhibited infection by HCoV-OC43, MERS-CoV, SARS-CoV, and the recently emerged SARS-CoV-2 (**Fig. 1d-g**). The antiviral effect of LY6E extended beyond human CoVs and blocked infection by the murine CoV murine hepatitis virus (MHV) (**Fig. 1h**). Given the zoonotic origin of SARS-CoV and MERS-CoV, both suspected to originate from bats, we next tested the antiviral potential of select LY6E orthologues. An alignment of LY6E orthologues of human, rhesus macaque, mouse, bat, and camel origin revealed strong conservation across species (**Extended Data Fig. 1b-c**). All LY6E orthologues inhibited HCoV-229E (**Extended Data Fig. 1d**). Recent surveillance of Kenyan camels, the main viral reservoir for MERS-CoV, indicates active circulation of the zoonotic CoV[13]. Human and camel LY6E restricted MERS-CoV infection (**Extended Data Fig. 1e**). To test the role of endogenous LY6E in controlling CoV infections, we used CRISPR-Cas9 gene editing to ablate LY6E expression in human lung adenocarcinoma cells (**Fig. 1i**). This cell line was selected as human hepatoma cells do not express LY6E irrespective of IFN treatment[9]. LY6E knockout (KO) cells were more susceptible to HCoV-229E (**Fig. 1j**). Reconstitution with a CRISPR-resistant LY6E variant (CR LY6E) restored antiviral activity in KO cells (**Fig. 1k-l**). Strikingly, the LY6E-mediated restriction in

3

hepatoma cells was largely specific to CoV. Among 10 genetically divergent viruses tested, only hepatitis C virus was also restricted (**Extended Data Fig. 1f**).

LY6E is a member of the LY6/uPAR family of GPI-anchored proteins, and is implicated in diverse cellular processes[14]. To evaluate the specificity of LY6E for inhibiting CoV, we ectopically expressed select LY6/uPAR proteins[9] and infected with HCoV-229E. Only LY6E inhibited CoV infection (**Extended Data Fig. 1g**). We previously showed that a conserved residue (L36) is required for LY6E-mediated enhancement of influenza A virus[9]. L36 was also required to restrict HCoV-229E infection (**Extended Data Fig. 1h**). These data suggest a conserved functional domain that is responsible for both the virus-enhancing and -restricting phenotypes.

Next, we investigated the effect of LY6E on specific steps of the virus replication cycle. First, we tested whether LY6E restricts HCoV-229E attachment to the cell surface and observed no effect (**Extended Data Fig. 2a**). In accordance, LY6E had no effect on surface expression of CD13, the specific receptor for HCoV-229E (**Extended Data Fig. 2b**). To test whether LY6E restricts viral entry, we used a vesicular stomatitis virus (VSV) pseudoparticle (pp) system bearing CoV spike (S) proteins. Strikingly, LY6E significantly inhibited VSVpp entry mediated by S proteins from HCoV-229E (**Fig. 2a**), MERS-CoV (**Fig. 2b**), SARS-CoV (**Fig. 2c**), and SARS-CoV-2 (**Fig. 2d**). Entry mediated by VSV glycoprotein G was only marginally impacted by LY6E (**Extended Data Fig. 2c, d**). To test whether LY6E interferes with the fusion of viral and cellular membranes, we performed a syncytia formation assay using propagation competent VSV pseudoviruses co-expressing CoV S protein and a GFP reporter (VSV*ΔG(CoV S)) (**Extended Data Fig. 3a**). LY6E potently inhibited CoV S protein-mediated syncytia formation (**Fig. 2e-f**). To determine whether LY6E impairs S protein expression or maturation, we also performed a heterologous syncytia formation assay. CoV-resistant hamster cells infected with trans-complemented GFP reporter VSV*ΔG(CoV) were co-cultured with susceptible target cells that ectopically expressed LY6E. LY6E again significantly blocked syncytia formation, demonstrating that LY6E inhibits S protein-mediated fusion and not S protein expression or maturation (**Extended Data Fig. 3b-c**). As membrane fusion can occur without syncytia formation, we also performed a quantitative fusion assay in which mixing of cell contents results in complementation of split luciferase (**Fig. 2g**).

4

Cells co-transfected with plasmids encoding CoV S proteins and split luciferase 1-7 were mixed with susceptible target cells co-expressing LY6E or vector control and split luciferase 8-11. LY6E reduced CoV S-mediated cell-cell fusion, indicating that LY6E blocks fusion of viral and cellular membranes (**Fig. 2h**). Time-course experiments revealed that LY6E had no effect on HCoV-229E translation, replication, assembly, or release (**Extended Data Fig. 2e-i**). Collectively, our results demonstrate that LY6E specifically inhibits CoV S protein-mediated membrane fusion, which is required for viral entry.

We next addressed whether LY6E modulates proteolytic activation of the S protein. Upon S protein-mediated binding to the respective receptor, host proteases cleave the S protein and make it fusion competent for "early entry" at the cell surface or "late entry" in endosomes[15,16]. Pharmacological inhibition of cell surface and endosomal proteases had no effect on LY6E-mediated restriction of CoV infection (**Extended Data Fig. 4a-c**). Next, we addressed whether LY6E directly interferes with the proteolytic activation of S protein. Mutation of S1/S2 and S2′ in the S protein prevents activation (**Extended Data Fig. 4d**)[16,17]. Ectopic LY6E expression had no effect on MERS-CoV S cleavage or infection by cleavage-resistant MERS-CoV pp (**Extended Data Fig. 4e-g**). Collectively, our data indicate that restriction of viral fusion is independent of S protein activation.

Next, we aimed to evaluate LY6E-mediated CoV restriction *in vivo*. Systemic genetic ablation of *Ly6e* in mice is embryonic lethal[18]. Therefore, we generated transgenic *Ly6e^{fl/fl}* mice, which are functionally 'wild-type (WT)' for Ly6e expression, and crossed them with *Vav1-iCre* mice to ablate *Ly6e* in cells that originate from a hematopoietic stem cell (HSC) progenitor (**Extended Data Fig. 5a-b**). This genetic model was chosen since immune cells are critical for protection from CoV *in vivo*[5,19-23]. Bone-marrow derived macrophages (BMDM) from *Ly6e^{ΔHSC}* mice had reduced *Ly6e* mRNA levels (**Extended Data Fig. 5c**). The natural mouse pathogen MHV is a well-studied model CoV that causes hepatitis and encephalomyelitis in mice[24]. *Ly6e^{ΔHSC}* BMDM were more susceptible to MHV infection than *Ly6e^{fl/fl}* BMDM, demonstrating that murine Ly6e is a restriction factor for murine CoV (**Extended Data Fig. 5d**).

To determine whether Ly6e is important for controlling CoV infection *in vivo*, *Ly6e^{fl/fl}* and *Ly6e^{ΔHSC}* mice were infected with a high dose (5 x 10^4 PFU) of MHV that causes sub-lethal hepatitis in WT

5

C57BL/6J mice[25]. Since MHV pathogenesis is influenced by sex[26], we performed independent experiments in male and female mice. *Ly6e$^{\Delta HSC}$* mice of both sexes rapidly succumbed to MHV infection by day 6 (**Fig. 3a-b**, **Extended Data Fig. 6a-b**). To examine viral pathogenesis and immunopathology in infected mice, *Ly6e$^{fl/fl}$* and *Ly6e$^{\Delta HSC}$* mice were infected with the same high dose of MHV and euthanized 3- or 5-days post-infection. At both time points, female *Ly6e$^{\Delta HSC}$* mice exhibited significantly higher levels of liver damage as measured by serum ALT while no difference was observed in male mice (**Fig. 3c,i**, **Extended Data Fig. 6c,i**). However, hepatic viral burden did not differ in either sex (**Fig. 3d,j**, **Extended Data Fig. 6d,j**), possibly due to tissue saturation at this high dose. Indeed, female but not male *Ly6e$^{\Delta HSC}$* mice exhibited increased liver damage and viral burden at a low dose (5 PFU) of MHV (**Extended Data Fig. 7a-b, f-g**). Spleen viral burden was elevated in female and male *Ly6e$^{\Delta HSC}$* mice at both time points and doses of MHV (**Fig. 3e,k**, **Extended Data Fig. 6e,k**, **Extended Data Fig. 7c,h**). At 3 days post-infection, there was no difference in liver necrosis, but inflammation was moderately reduced in female but not male *Ly6e$^{\Delta HSC}$* mice (**Fig. 3f-h**, **Extended Data Fig. 6f-h**). By 5 days post-infection and at both low and high doses of MHV, female *Ly6e$^{\Delta HSC}$* mice had significantly higher levels of liver necrosis and a reduced presence of mononuclear immune cells (**Fig. 3l-n**, **Extended Data Fig. 7d-e**), whereas no difference was observed in male mice (**Extended Data Fig. 6l-n**, **Extended Data Fig. 7i-j**). Liver damage in *Ly6e$^{\Delta HSC}$* mice was further corroborated at an intermediate viral dose (5 x 10^3 PFU), which resulted in visibly apparent brittleness, pallor, and necrotic foci (**Extended Data Fig. 7k-n**). These data demonstrate that Ly6e in hematopoietic cells is important for controlling murine CoV infection.

We next used a transcriptomic approach to evaluate the effect of *Ly6e* ablation on global gene expression in liver and spleen of female *Ly6e$^{fl/fl}$* and *Ly6e$^{\Delta HSC}$* mice injected with PBS or the high dose of MHV at 3- and 5- days post-infection. In infected tissues, loss of *Ly6e* in hematopoietic cells correlated with differential gene expression in pathways associated with tissue damage, such as liver-specific metabolic genes, angiogenesis, wound healing, and immune response to viruses (**Fig. 4a-c**). We also observed a striking loss of genes associated with the type I IFN response, inflammation, antigen presentation, and B cells in infected *Ly6e$^{\Delta HSC}$* mice (**Fig. 4d-e**, **Extended Data Fig. 8**).

The histopathology (**Fig. 3h,n**) and transcriptome data (**Fig 4a-e**, **Extended Data Fig. 8**) prompted us to determine how loss of *Ly6e* affects immune cell numbers during infection. Absolute numbers of different immune cell subsets were quantified from *Ly6e^{ΔHSC}* and *Ly6e^{fl/fl}* mice 5 days after injection with PBS or the intermediate dose of MHV (**Extended Data Fig. 7k-n**, **Extended Data Fig. 9**). Multiple cell types were depleted in livers and spleens of infected *Ly6e^{ΔHSC}* mice, irrespective of sex (**Figure 4f-g, Extended Data Fig. 10a-b**). B cells were dramatically reduced in livers from infected *Ly6e^{ΔHSC}* mice. Hepatic CD4$^+$ T cells, NK cells, dendritic cells (DC), macrophages, and neutrophils were also depleted in infected *Ly6e^{ΔHSC}* mice, whereas CD8$^+$ T cells were unchanged (**Fig. 4f**, **Extended Data Fig. 10a)**. Infected *Ly6e^{ΔHSC}* mice had a reduction in all splenic immune cell subsets except for CD4$^+$ and CD8$^+$ T cells (**Fig. 4g**, **Extended Data Fig. 10b**). Depletion of immune cell populations in *Ly6e^{ΔHSC}* organs was MHV-dependent, as cell numbers were not altered in PBS-injected mice.

To determine whether loss of immune cells in MHV-infected *Ly6e^{ΔHSC}* mice correlates with increased permissiveness to infection, we assessed MHV infection in splenocytes cultured from *Ly6e^{ΔHSC}, Ly6e^{fl/fl},* and *Ifnar^{-/-}* mice. In *Ly6e^{fl/fl}* splenocyte cultures, MHV infected macrophages, neutrophils, DC, and B cells, but not CD4$^+$ or CD8$^+$ T cells, as previously published (**Fig. 4h**, **Extended Data Fig. 10c**)[23]. Strikingly, B cells from both male and female *Ly6e^{ΔHSC}* mice were highly susceptible to MHV infection when compared to B cells from *Ly6e^{fl/fl}* or *Ifnar^{-/-}* mice. DC from female *Ly6e^{ΔHSC}* mice were also more susceptible to MHV infection. Surprisingly, no other cell type demonstrated a strong Ly6e-dependent susceptibility to MHV infection.

Together, our data demonstrate an important role for Ly6e in immune cell-mediated control of CoV infection. Higher viral burden and lower liver inflammation suggests that liver damage in MHV-infected female *Ly6e^{ΔHSC}* mice may be due to viral pathogenesis that exceeds the ability of the immune system to control the infection. Notably, we observed MHV-induced loss of three classes of cells: 1) cells that are not permissive to the virus (CD4$^+$ T cells), 2) cells that are permissive to MHV but do not demonstrate Ly6e KO-dependent infection (NK cells, macrophages, and neutrophils), and 3) cells that are permissive to MHV in a Ly6e KO-dependent manner (B cells and DC). This latter group is capable of antigen-presentation to CD4$^+$ T cells[27,28]. Thus, in the absence of Ly6e, unrestricted MHV infection

of B cells or DC may impair T cell priming, thereby negatively impacting recruitment and activation of NK cells, macrophages, and neutrophils that contribute to control of viral disease.

In conclusion, we identified LY6E as a pan CoV restriction factor that limits CoV entry and protects the host from severe viral disease. Our findings are striking given that LY6E has been primarily associated with an enhancing phenotype in which LY6E promotes entry of multiple viruses[29]. However, our data clearly expand the role of LY6E during coronaviral infection and establishes a novel function in protecting the host immune cell compartment. Determining the precise molecular mechanism underlying how LY6E inhibits CoV S protein-mediated membrane fusion will advance our understanding of cellular antiviral defenses against these important human pathogens. Antiviral membrane fusion inhibitors have been successfully implemented for treatment of HIV-1 infection[30]. A therapeutic approach mimicking the mechanism of action of LY6E could provide a first line of defense against novel emerging CoV infections. Furthermore, delineating which Ly6e-expressing immune cells protect mice from MHV will provide new insight into how individual antiviral effectors in distinct cellular compartments modulate viral pathogenesis.

References

1   Zhu, N. *et al.* A Novel Coronavirus from Patients with Pneumonia in China, 2019. *N Engl J Med*, doi:10.1056/NEJMoa2001017 (2020).

2   Kindler, E., Thiel, V. & Weber, F. Interaction of SARS and MERS Coronaviruses with the Antiviral Interferon Response. *Adv Virus Res* **96**, 219-243, doi:10.1016/bs.aivir.2016.08.006 (2016).

3   Corman, V. M., Muth, D., Niemeyer, D. & Drosten, C. Hosts and Sources of Endemic Human Coronaviruses. *Adv Virus Res* **100**, 163-188, doi:10.1016/bs.aivir.2018.01.001 (2018).

4   Wang, B. X. & Fish, E. N. Global virus outbreaks: Interferons as 1st responders. *Semin Immunol* **43**, 101300, doi:10.1016/j.smim.2019.101300 (2019).

5   Cervantes-Barragan, L. *et al.* Control of coronavirus infection through plasmacytoid dendritic-cell-derived type I interferon. *Blood* **109**, 1131-1137, doi:10.1182/blood-2006-05-023770 (2007).

6   Schoggins, J. W. Interferon-Stimulated Genes: What Do They All Do? *Annu Rev Virol* **6**, 567-584, doi:10.1146/annurev-virology-092818-015756 (2019).

7   Schoggins, J. W. *et al.* A diverse range of gene products are effectors of the type I interferon antiviral response. *Nature* **472**, 481-485, doi:10.1038/nature09907 (2011).

8   Dittmann, M. *et al.* A serpin shapes the extracellular environment to prevent influenza A virus maturation. *Cell* **160**, 631-643, doi:10.1016/j.cell.2015.01.040 (2015).

9   Mar, K. B. *et al.* LY6E mediates an evolutionarily conserved enhancement of virus infection by targeting a late entry step. *Nature Communications* **9**, 3603, doi:10.1038/s41467-018-06000-y (2018).

10   Hackett, B. A. & Cherry, S. Flavivirus internalization is regulated by a size-dependent endocytic pathway. *Proc Natl Acad Sci U S A* **115**, 4246-4251, doi:10.1073/pnas.1720032115 (2018).

11   Yu, J., Liang, C. & Liu, S. L. Interferon-inducible LY6E Protein Promotes HIV-1 Infection. *J Biol Chem* **292**, 4674-4685, doi:10.1074/jbc.M116.755819 (2017).

12   Yu, J., Liang, C. & Liu, S. L. CD4-Dependent Modulation of HIV-1 Entry by LY6E. *J Virol* **93**, doi:10.1128/JVI.01866-18 (2019).

13   Sikkema, R. S. *et al.* Global status of Middle East respiratory syndrome coronavirus in dromedary camels: a systematic review. *Epidemiol Infect* **147**, e84, doi:10.1017/S095026881800345X (2019).

14   Upadhyay, G. Emerging Role of Lymphocyte Antigen-6 Family of Genes in Cancer and Immune Cells. *Front Immunol* **10**, 819, doi:10.3389/fimmu.2019.00819 (2019).

15   Heald-Sargent, T. & Gallagher, T. Ready, set, fuse! The coronavirus spike protein and acquisition of fusion competence. *Viruses* **4**, 557-580, doi:10.3390/v4040557 (2012).

16   Park, J. E. *et al.* Proteolytic processing of Middle East respiratory syndrome coronavirus spikes expands virus tropism. *Proc Natl Acad Sci U S A* **113**, 12262-12267, doi:10.1073/pnas.1608147113 (2016).

17   Kleine-Weber, H., Elzayat, M. T., Hoffmann, M. & Pohlmann, S. Functional analysis of potential cleavage sites in the MERS-coronavirus spike protein. *Sci Rep* **8**, 16597, doi:10.1038/s41598-018-34859-w (2018).

18   Langford, M. B., Outhwaite, J. E., Hughes, M., Natale, D. R. C. & Simmons, D. G. Deletion of the Syncytin A receptor Ly6e impairs syncytiotrophoblast fusion and placental morphogenesis causing embryonic lethality in mice. *Sci Rep* **8**, 3961, doi:10.1038/s41598-018-22040-2 (2018).

19   Matthews, A. E. *et al.* Antibody is required for clearance of infectious murine hepatitis virus A59 from the central nervous system, but not the liver. *J Immunol* **167**, 5254-5263, doi:10.4049/jimmunol.167.9.5254 (2001).

20   Phares, T. W. *et al.* CD4 T cells promote CD8 T cell immunity at the priming and effector site during viral encephalitis. *J Virol* **86**, 2416-2427, doi:10.1128/JVI.06797-11 (2012).

21   Wijburg, O. L., Heemskerk, M. H., Sanders, A., Boog, C. J. & Van Rooijen, N. Role of virus-specific CD4+ cytotoxic T cells in recovery from mouse hepatitis virus infection. *Immunology* **87**, 34-41 (1996).

22   Wijburg, O. L., Heemskerk, M. H., Boog, C. J. & Van Rooijen, N. Role of spleen macrophages in innate and acquired immune responses against mouse hepatitis virus strain A59. *Immunology* **92**, 252-258, doi:10.1046/j.1365-2567.1997.00340.x (1997).

23   Cervantes-Barragan, L. *et al.* Type I IFN-mediated protection of macrophages and dendritic cells secures control of murine coronavirus infection. *J Immunol* **182**, 1099-1106 (2009).

24   Weiss, S. R. & Leibowitz, J. L. Coronavirus pathogenesis. *Adv Virus Res* **81**, 85-164, doi:10.1016/B978-0-12-385885-6.00009-2 (2011).

25   Eriksson, K. K., Cervantes-Barragan, L., Ludewig, B. & Thiel, V. Mouse hepatitis virus liver pathology is dependent on ADP-ribose-1"-phosphatase, a viral function conserved in the alpha-like supergroup. *J Virol* **82**, 12325-12334, doi:10.1128/JVI.02082-08 (2008).

26   Karnam, G. *et al.* CD200 receptor controls sex-specific TLR7 responses to viral infection. *PLoS Pathog* **8**, e1002710, doi:10.1371/journal.ppat.1002710 (2012).

27   Hong, S. *et al.* B Cells Are the Dominant Antigen-Presenting Cells that Activate Naive CD4(+) T Cells upon Immunization with a Virus-Derived Nanoparticle Antigen. *Immunity* **49**, 695-708 e694, doi:10.1016/j.immuni.2018.08.012 (2018).

28   Mempel, T. R., Henrickson, S. E. & Von Andrian, U. H. T-cell priming by dendritic cells in lymph nodes occurs in three distinct phases. *Nature* **427**, 154-159, doi:10.1038/nature02238 (2004).

29   Yu, J. & Liu, S. L. Emerging Role of LY6E in Virus-Host Interactions. *Viruses* **11**, doi:10.3390/v11111020 (2019).

30   Lalezari, J. P. *et al.* Enfuvirtide, an HIV-1 fusion inhibitor, for drug-resistant HIV infection in North and South America. *N Engl J Med* **348**, 2175-2185, doi:10.1056/NEJMoa035026 (2003)
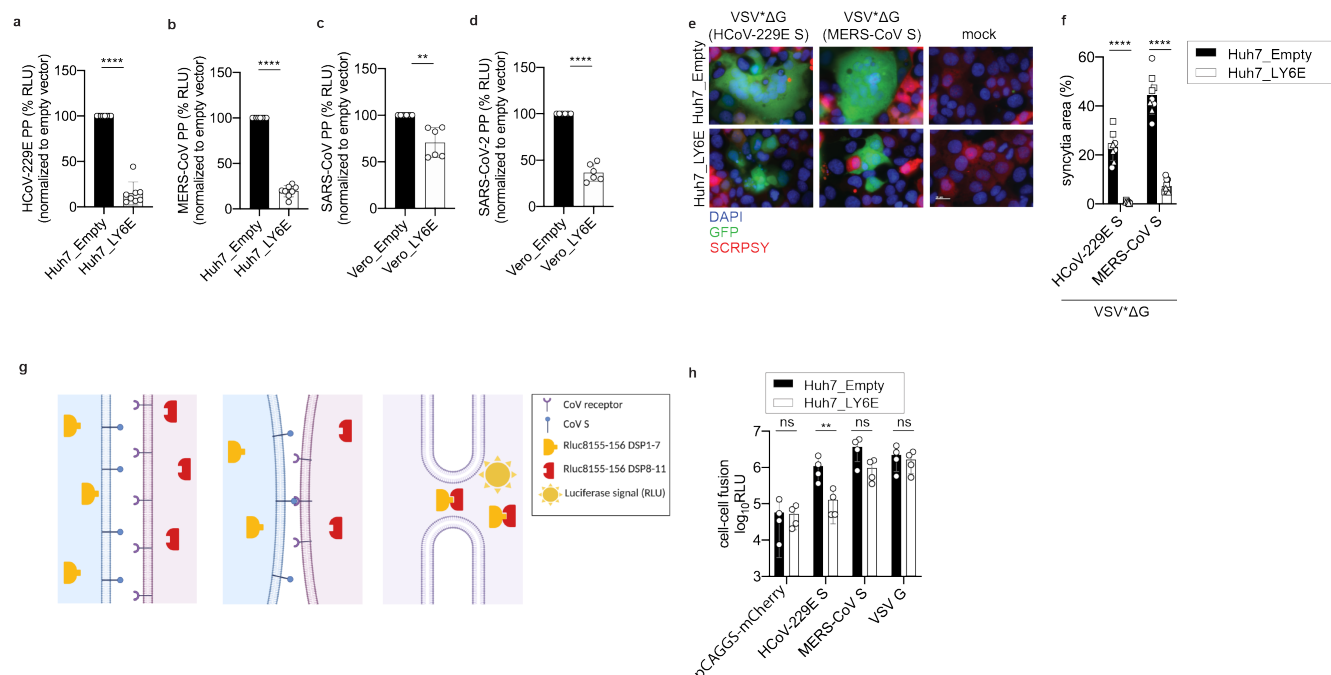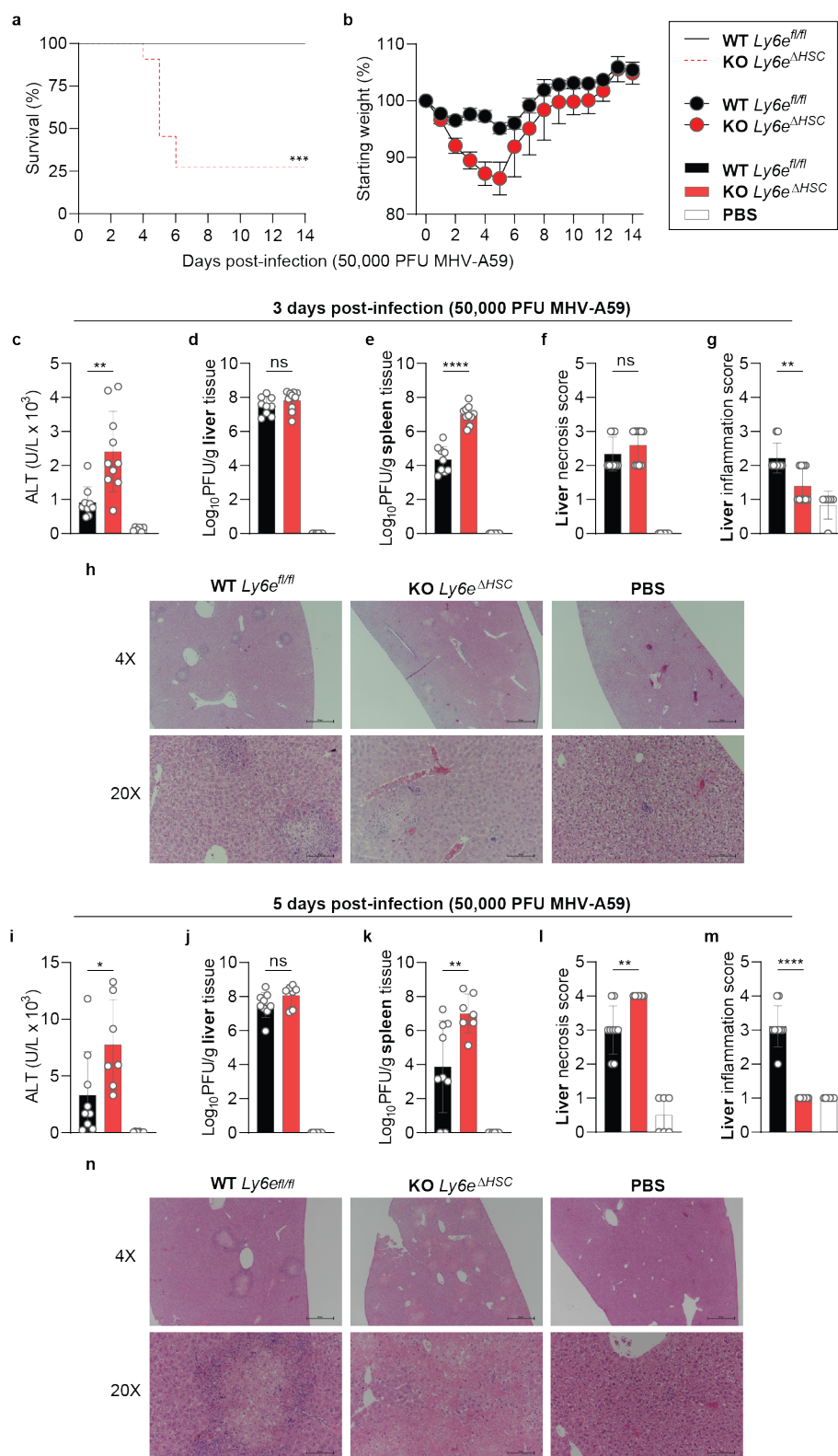
Figures
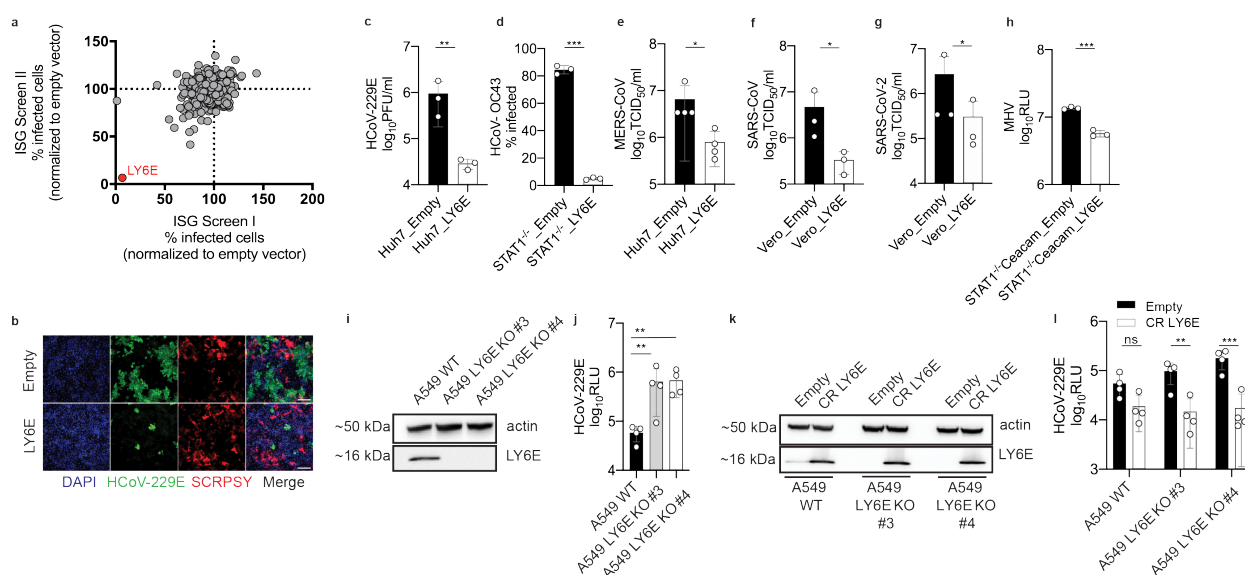
Figure 1. ISG screen identifies LY6E as a potent coronavirus restriction factor. a, Duplicate screens depicting HCoV-229E infection (24 hours post-infection) in Huh7 cells ectopically expressing ISGs. **b**, HCoV-229E infection of Huh7 cells expressing LY6E or control vector (Empty). Blue: DAPI, green: HCoV-229E N protein, red: TagRFP encoded in SCRPSY vector. **c-h**, Effect of LY6E expression on diverse coronaviruses. Stably transduced cells were infected with HCoV-229E (**c**), HCoV-OC43 (**d**), MERS-CoV (**e**), SARS-CoV (**f**), SARS-CoV-2 (**g**), MHV-Gluc (**h**). **i**, Western blot of WT A549 or two LY6E KO clones (#3, #4). **j**, HCoV-229E infection of WT or LY6E KO A549. **k**, Western blot of WT or LY6E KO A549 reconstituted with CRISPR-resistant LY6E (CR LY6E) or control vector (Empty). **l**, HCoV-229E infection of CR LY6E-reconstituted WT or LY6E KO A549. Viral replication readouts included: titer determination by plaque assay (**c**), infectivity by nucleoprotein staining and quantitation by flow cytometry (**d**), limiting dilution assay (**e,f,g**), luciferase activity shown as relative light units (RLU) (**h,j,l**). Data represent average of independent biological replicates, n=3 (**c-d,f-h**), n=4 (**e,j,l**). In **b**, scale bars are 200 μM. Statistical significance was determined by unpaired student's t-test with Welch's correction (**c-d**, **f-g**), one-tailed Mann-Whitney U test (**e**), ratio paired student's t-test (**g**), 2way ANOVA followed by Sidak's or Dunnett's multiple comparison test (**j,l**). Error bars: SD. *P* values: **c**, ** p=0.0088; **d**, *** p=0.0001; **e**, * p=0.0143; **f**, * p=0.0286; **g**, * p=0.0101; **h**, *** p=0.0010; **j**, ** p=0.0073, p=0.0033; **l**, ns=0.0740, ** p=0.0013, *** p=0.0001.

12

Figure 2. LY6E inhibits viral membrane fusion and syncytia formation. a-d, VSV pseudoparticles (PP) harboring spike proteins from HCoV-229E (**a**), MERS-CoV (**b**), SARS-CoV (**c**), SARS-CoV-2 (**d**) were inoculated on LY6E- or empty vector-expressing cells. Virus entry efficiency was quantified by measuring virus-encoded luciferase reporter activity. **e**, VSV pseudoparticles expressing VSV G protein on their surface and encoding CoV S protein and GFP (VSV*ΔG(CoV S)) were inoculated with LY6E- or empty vector-expressing Huh7. Syncytia formation was analyzed by immunofluorescence microscopy. Blue: DAPI, green: GFP, red: TagRFP inserted in SCRPSY vector. **f**, Quantification of VSV*ΔG(CoV S) induced syncytia depicted as percentage syncytia area. Three independent areas were analyzed per biological replicate (circle, square, triangle). **g**, Schematic depiction of the cell-cell fusion assay created with BioRender. **h**, Cell-cell fusion was measured by co-incubating cells transfected with plasmids encoding CoV S proteins and a split-luciferase construct (DSP1-7) together with CoV permissive LY6E-expressing or control cells transfected with the second fragment of split-luciferase (DSP8-11). Data represent averages of independent biological replicates, n=8 (**a,b**), n=6 (**c,d**), n=3 (**f**), n=4 (**h**). Statistical significance was determined by unpaired student's t-test with Welch's correction (**a-d**) and 2way ANOVA followed by Sidak's multiple comparison test (**f,h**). Outliers were removed using Grubbs outlier test (**a**). In **e**, scale bar is 20 μM. Error bars: SD. *P* values: **a**, **** p=<0.0001; **b**, ****

p=<0.0001; **c**, **p=0.0066; **d**, **** p=<0.0001; **f**, **** p=<0.0001; **h**, ns p=0.9975, ** p=0.0054, ns

p=0.1520, 0.9892.

p=<0.0001; **c**, **p=0.0066; **d**, **** p=<0.0001; **f**, **** p=<0.0001; **h**, ns p=0.9975, ** p=0.0054, ns

p=0.1520, 0.9892.

Figure 3. *Ly6e^ΔHSC* mice are more susceptible to murine hepatitis virus. a-b, Female *Ly6e^fl/fl* and *Ly6e^ΔHSC* mice were injected with PBS or MHV and monitored for survival (**a**) and weight loss (**b**). **c-n**, Mice were assessed at 3 (**c-h**) or 5 (**i-n**) days post-infection for serum ALT (**c,i**), viral titers in liver (**d,j**) and spleen (**e,k**), and liver necrosis and inflammation (**f-h, l-n**). For **a-b**, n=13 for days 0-14 (*Ly6e^fl/fl*), n=11 for day 0-3, n= 10 for days 4-5, n=5 for days 5-6, n=3 for days 6-14 (*Ly6e^ΔHSC*) from

15

three pooled experiments. For **c-g**, n=9 (*Ly6e*$^{fl/fl}$), n=10 (*Ly6e*$^{\Delta HSC}$), n=6 (PBS) from two pooled experiments. For **i-m**, n=9 (*Ly6e*$^{fl/fl}$,), n=7 (*Ly6e*$^{\Delta HSC}$), n=6 (PBS) from two pooled experiments. In **h,n**, scale bars are 500 μM (4x) and 100 μM (20x). Statistical significance was determined by Mantel-Cox test (**a**), two-tailed unpaired student's t-test with Welch's correction (**c-e**, **i-k**), two-tailed Mann-Whitney U test (**f-g**, **l-m**). Error bars: SEM (**b**), SD (**c-g**, **i-m**). *P* values: **a**, *** p=0.0002; c, ** p=0.0031; **d**, ns p=0.2136; **e**, **** p=5.759 x 10^{-7}; **f**, ns p=0.3698; **g**, ** p=0.0054; **i**, * p=0.0430; **j**, ns p=0.1321; **k**, ** p=0.0094; **l**, ** p=0.0072; **m**, **** p=8.741 x 10^{-5}.
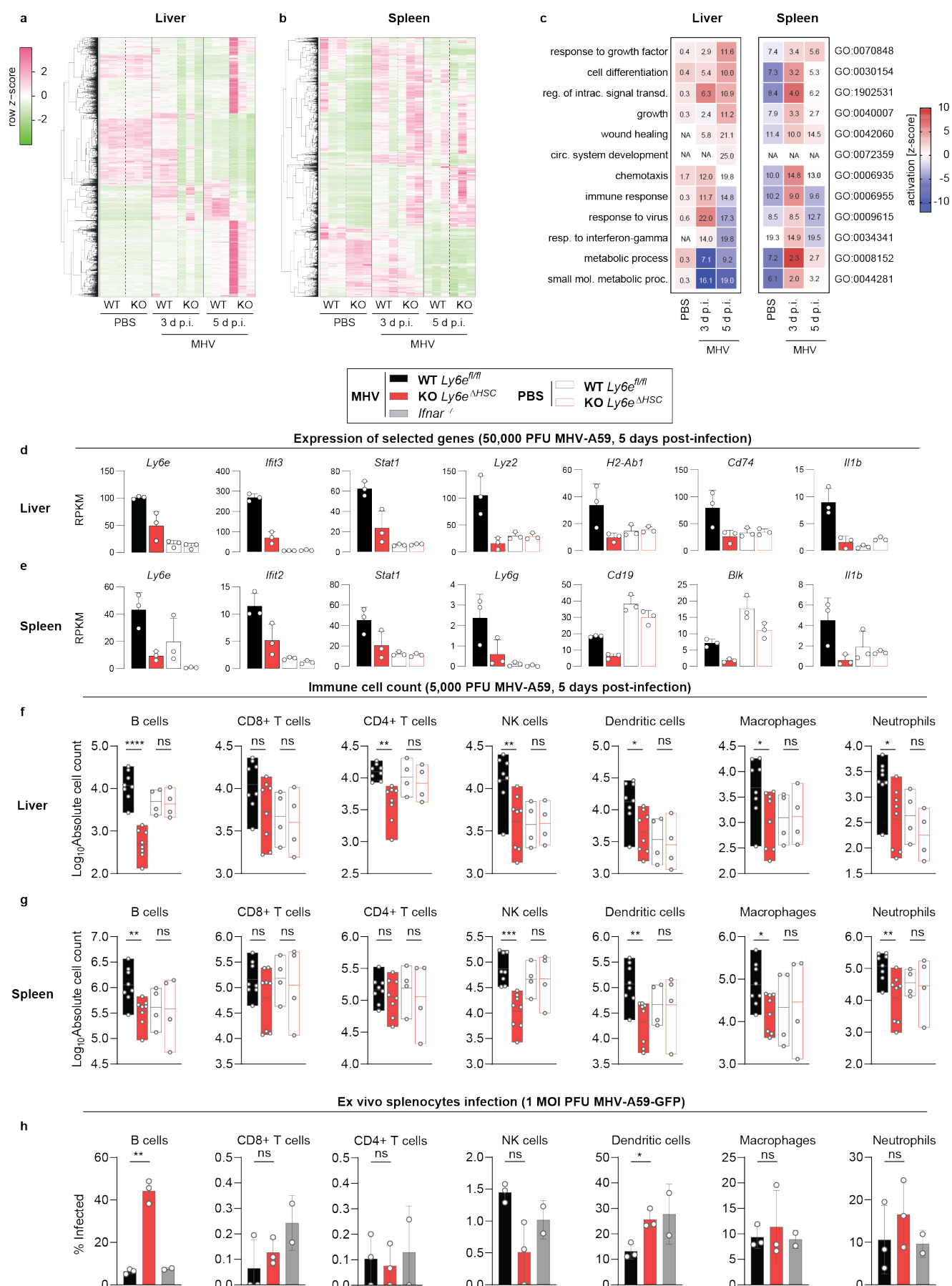
Figure 4. Murine hepatitis virus infection alters hepatic and splenic immune responses in female

Ly6e^ΔHSC **mice. a-e**, Transcriptomic analysis from *Ly6e^fl/fl* (WT) and *Ly6e^ΔHSC* (KO) mice. **a-b**, Heat

maps displaying significant changes (mean RPKM > 0.5; fold change > 2; FDR ≤ 0.05) in liver (**a**) and spleen (**b**). Dendrograms are normalized read data (row z-score) clustered with complete linkage method employing Spearman Rank correlation distance measurement. **c**, Pathway analysis of KO versus WT. Up- (red) or down-regulated (blue) pathways indicated by activation z-score. Numbers show significantly dysregulated genes as percentage of total gene number included in pathway. **d-e**, Expression of select genes in liver (**d**) and spleen (**e**). **f-g**, Immune cell counts from liver (**f**) and spleen (**g**). **h**, Infection of cultured splenocytes. For **a-e**, n=3. For **f-g**, n=8 MHV-injected, n=4 PBS-injected from two pooled experiments. For **h**, n=3 (*Ly6e$^{fl/fl}$* and *Ly6e$^{\Delta HSC}$*) or n=2 (*Ifnar$^{-/-}$*) from two pooled experiments. Significance for **f-h** was determined by two-tailed unpaired student's t-test with Welch's correction. Error bars: SD (**d-h**). *P* values (left-right): **f**, **** p=1.3644 x 10^{-6}, ns p=0.7952, ns p=0.0781, ns p=0.7732, ** p=0.0016, ns p=0.6261, ** p=0.0068, ns p=0.9494, * p=0.0141, ns p=0.7639, * p=0.0436, ns p=0.9600, * p=0.0174, ns p=0.3096; **g,** ** p=0.0052, ns p=0.9447, ns p=0.1579, ns p=0.7769, ns p=0.4104, ns p=0.6924, *** p=1.754 x 10^{-4}, ns p=0.9842, ** p=0.0034, ns p=0.9848, * p=0.0169, ns p=0.8591, ** p=0.0076, ns p=0.8623; **h,** ** p=0.0051, ns p=0.4525, ns p=0.7379, ns p=0.0702, * p=0.0119, ns p=0.6787, ns p=0.4112.

18

Methods

Viruses

Recombinant HCoV-229E[31], HCoV-229E-Rluc (expressing Renilla luciferase [Rluc] by replacing the majority of HCoV-229E ORF4)[32], HCoV-OC43[33], MHV strain A59[34], MHV-Gluc, strain A59 (expresses a Gaussia luciferase [Gluc] replacing accessory gene 4)[35], MHV-GFP strain A59[25], MERS-CoV strain EMC[36], and SARS-CoV strain Frankfurt-1[37] have been described previously. SARS-CoV-2 (BetaCoV/Wuhan/IVDC-HB-01/2019, GISAID Accession ID: EPI_ISL_402119) stocks were propagated on VeroE6 cells. HCoV-229E viruses were propagated on Huh-7 cells, MERS-CoV and SARS-CoV were propagated on VeroB4 cells, HCoV-OC43 was propagated on HCT-8 cells[38], and MHV stocks were propagated on 17Cl1 cells. Lentivirus particles using the SCRPSY lentiviral backbone were generated as described previously[7,8].

VSV*ΔG(Fluc) (G glycoprotein-deficient VSV encoding green fluorescent protein [GFP] and firefly luciferase [Fluc]) was generated as described previously and was propagated on BHK-G43 cells[39].

The generation of viral stocks for the following viruses has been previously described: hPIV-3-GFP[40] (based on strain JS, generously provided by P.L. Collins), RSV-GFP[41] (based on strain A2, generously provided by P.L. Collins), YFV-Venus[42] (derived from YF17D-5′C25Venus2AUbi), DENV-GFP[43] (derived from IC30P-A, a full-length infectious clone of strain 16681), WNV-GFP[44] (derived from pBELO-WNV-GFP-RZ, generously provided by I. Frolov), HCV-Ypet[45] (based on the chimeric Jc1 virus of strains: J6 and JFH-1), SINV-GFP[46] (derived from pS300/pS300-GFP, generously provided by M.T. Heise), VEEV-GFP[47] (derived from pTC83-GFP infectious clone, generously provided by I. Frolov), CHIKV-GFP[48] (derived from pCHIKV-LR 5′GFP, generously provided by S. Higgs). ZIKV (PRVABC59, obtained from the CDC, Ft. Collins) was amplified and titrated as described previously[49].

Viral infection assays

HCoV-229E: 1.5×10^5 stable LY6E expressing or control cells were seeded in a 12-well plate and infected with HCoV-229E in a serial dilution. Cells were incubated for 2 hours at 33°C, then viral supernatant was removed, and an overlay of 1:1 Avicel (2.4%) (Avicel RC-581NF) and 2x DMEM,

supplemented with 10% FBS and 1x penicillin/streptomycin (p-s), was added. Cells were incubated for 3 days at 33°C before medium was removed, cells were washed, and stained with crystal violet (Sigma-Aldrich). Plaque forming units (PFU) were calculated.

HCoV-OC43: 5.0 x 10^4 stable LY6E expressing or control cells were seeded in a 24-well plate and infected at 33°C for 1 hour with HCoV-OC43 (MOI=1). Virus was aspirated and 10% FBS/1x NEAA/1x p-s/RPMI (cRPMI) was added back to cells. 24 hours post-infection, cells were dissociated using Accumax (Sigma-Aldrich), fixed in 1% PFA, permeabilized per manufacturer's protocol (BD Cytofix/Cytoperm), and stained for nucleoprotein (1:500) and a goat anti-mouse AlexaFluor488-conjugated secondary antibody (1:2000). Infection was analyzed by flow cytometry.

MERS-CoV/ SARS-CoV/ SARS-CoV-2: 1 x 10^4 stable LY6E expressing or control cells were seeded in a 96-well plate and infected at 37°C in a serial dilution assay. 3-4 days post-infection supernatant was removed, and cells were stained with crystal violet (Sigma-Aldrich). Cytopathic effect (CPE) was determined upon visual inspection and $TCID_{50}$/ml calculated according to the Reed and Muench method. MHV-Gluc: 1 x 10^5 stable LY6E expressing or control cells were seeded in a 24-well plate and infected with MHV-Gluc (MOI=0.1) at 37°C. After 2 hours, virus inoculum was removed, cells were washed with PBS, and cRPMI added back. 24 hours post-infection, cell culture supernatant was harvested, and Gluc activity was measured using Pierce Gaussia Luciferase Glow Assay Kit (ThermoFisher Scientific) and a plate luminometer (EnSpire 2300 Multilabel reader by Perkin Elmer). For testing the virus panel against LY6E, 1 x 10^4 stable LY6E expressing or control Huh7.5 cells were seeded in a 96-well plate. Cells were infected with the following viruses and harvested after the indicated time: HCoV-229E (MOI=0.001, 72 hours), HCV-Ypet (MOI=1, 72 hours), CHIKV-GFP (MOI=0.005, 24 hours), hPIV-3-GFP (MOI=0.015, 24 hours), RSV-GFP (MOI=1.5, 24 hours), SINV-GFP (MOI=0.1, 24 hours), VEEV-GFP (MOI=0.0075, 24 hours), WNV-GFP (MOI=1.5, 24 hours), ZIKV PRVABC59 (MOI=0.01, 48 hours), YFV 17D-venus (MOI=0.01, 48 hours) and DENV-GFP (MOI=0.05, 72 hours). At the indicated time points, cells were fixed with 4% paraformaldehyde (PFA)/PBS. ZIKV-infected cells were stained for viral E protein and an AlexaFluor488-conjugated goat

20

anti-mouse secondary antibody. Images were acquired with a fluorescence microscope and analyzed using ImageXpress Micro XLS (Molecular Devices, Sunnyvale, CA).

HCoV-229E-Rluc infection assay of KO cells

For infection assays, 1 x 10^5 target cells were seeded in a 24-well plate one day prior infection. Cells were infected with HCoV-229E-Rluc (MOI 0.1) in OptiMEM (Gibco) for 2 hours at 33°C. Cells were washed 1x with PBS and 10% FBS/1x NEAA/1x p-s/DMEM (cDMEM) was added back. Cells were incubated at 33°C for 24 hours, then washed with PBS and lysed using the Renilla Luciferase Assay System kit (Promega). Rluc activity was measured using a plate luminometer (EnSpire 2300 Multilabel reader by Perkin Elmer). For the reconstitution with CRISPR resistant LY6E (CR LY6E), 2.5 x 10^4 cells were seeded in a 24-well plate. One day post-seeding, cells were either left untransduced or transduced with a lentiviral vector encoding for CR LY6E or the empty control. 48 hours post-transduction, cell lysates were either infected with HCoV-229E-Rluc (MOI=0.1) for 24 hours as described above or harvested for Western blot.

VSV pseudoparticles

Pseudotyping of VSV*ΔG(Fluc) was performed as previously described[50]. Briefly, 6 x 10^5 293LTV cells were seeded in a 6-well plate and transfected using Lipofectamine 2000 (Invitrogen) which was complexed with DNA plasmids driving the expression of either VSV G protein (positive control), the respective CoV S proteins, or the fluorophore mCherry (negative control). Expression vectors for vesicular stomatitis virus (VSV, serotype Indiana) glycoprotein (VSV-G, Genbank accession number: NC_001560), HCoV-229E S (pCAGGS-229E S, Genbank accession number: X16816), MERS-CoV S (pCAGGS-MERS S, Genbank accession number: JX869059 with silent point mutation (C4035A, removing internal XhoI), SARS-CoV S (pCAGGS-SARS S, Genbank accession number: AY291315.1 with two silent mutation (T2568G, T3327C)), have been described previously[51-53]. The expression plasmid for SARS-CoV-2 was generated as follows: the coding sequence of a synthetic, codon-optimized (for human cells) SARS-CoV-2 DNA (GeneArt Gene Synthesis, Thermo Fisher Scientific)

21

based on the publicly available protein sequence in the National Center for Biotechnology Information database (NCBI Reference Sequence: YP_009724390.1) was PCR-amplified and cloned into the pCG1 expression vector between BamHI and XbaI restriction sites. The MERS-CoV S cleavage mutants have been described before[17]. pCAGGS_mCherry was generated upon cloning of the mCherry reporter gene into the pCAGGS expression vector (primer sequences and cloning procedure are available upon request). At 20 hours post-transfection, cells were infected with VSV-G-trans-complemented VSV*ΔG(FLuc) (MOI=5) for 30 minutes at 37°C, washed with PBS, and further incubated for 1 hour in cDMEM that was supplemented with Mab I1 (ATCC), a neutralizing monoclonal antibody directed to the VSV G protein. Cells were then washed and cDMEM was added back. Viral supernatant was harvested at 16 – 24 hours post-infection. Cellular debris was removed by centrifugation (3,000 × g for 10 minutes) and used to inoculate 2 x 10^4 target cells in a 96-well plate (6 technical replicates). Cells were incubated for 16–18 hours at 37°C before Fluc activity in cell lysates was detected using a plate luminometer (EnSpire 2300 Multilabel reader by Perkin Elmer) and the Bright-Glo Luciferase Assays System (Promega). Experiments with pseudotyped SARS-CoV and SARS-CoV-2 were performed as previously described[17].

Split luciferase fusion assay

The split luciferase fusion assay has been described before, with slight modifications[54]. Briefly, 6 x 10^5 293LTV cells were transfected with plasmids encoding CoV S proteins (pCAGGS-HCoV-229E, pCAGGS-MERS-CoV) together with a split-luciferase construct (Rluc8155-156 DSP1-7). The empty expression plasmid (pCAGGS-mCherry) as well as a construct encoding for VSV G served as negative and positive control, respectively. 2 x 10^5 stable LY6E expressing or empty control Huh7 cells were transfected using Lipofectamine 2000 (Thermo Fisher Scientific) with a plasmid encoding the second half of the split-luciferase protein (Rluc8155-156 DSP8-11). Approximately 30 hours post-transfection, both cell populations were dissociated (TryPLE Express, Gibco), counted, and equal cell numbers (2x10^4 cells each) were co-cultured for 16 – 20 hours at 37°C. Supernatant was harvested and cells lysed using ice-cold passive lysis buffer (Promega). Cells were immediately transferred to -80°C for at least

1 hour, before Rluc activity was determined using the Renilla Luciferase Assay System (Promega). Cells were kept on ice during all times post-cell lysis to eliminate DSP post-lysis complementation.

Generation of recombinant VSV vector driving CoV S protein expression (VSV*ΔG(CoV))

Following extraction of total RNA from MERS-CoV (strain EMC) infected VeroE6 cells, the cDNA encoding the MERS-CoV S protein was generated by reverse transcription (RevertAid Premium Reverse Transkriptase, ThermoScientific). Three overlapping cDNA fragments were amplified by PCR (Phusion Hot Start II High Fidelity Polymerase, Thermo Scientific) and subsequently assembled by overlapping PCR. The cDNAs encoding the S proteins of either MERS-CoV (strain EMC) or HCoV-229E (truncated variant lacking the 10 amino acids at the C terminus, original plasmid pCAGGS-229E S) were amplified by PCR and inserted into the pVSV* plasmid[55] between MluI and BstEII restriction sites. The resulting plasmids were used to generate the recombinant viruses VSV*ΔG(MERS S) and VSV*ΔG(229E S) according to a published procedure[56]. All viruses were propagated on BHK-G43 cells[57], resulting in viruses predominantly containing the homotypic VSV glycoprotein G in the envelope.

Syncytia formation assay

Cells expressing LY6E or empty control were infected with VSV*ΔG(MERS S) or VSV*ΔG(229E S) at a MOI of 0.01. At 20 hours post-infection, the cells were fixed with 3% PFA/PBS and the nuclei stained with 4',6-diamidine-2'-phenylindole (DAPI, Sigma). An inverted fluorescence microscope (Zeiss) was used to determine area percentage area covered by syncytia.

For heterologous cell-cell fusion assay, BHK-21 cells were infected with VSV*ΔG(CoV S) at a MOI of 1. After 2 hours, the cells were treated with trypsin/EDTA (Life Technologies, Zug, Switzerland) and resuspended in DMEM supplemented with 5% FBS (2×10^4 cells/mL). The infected BHK-21 cell suspension (500 µL) was seeded into 24-well cell culture plates along with LY6E- or empty control-expressing Huh7 (1×10^4 cells). Cell co-cultures were incubated for 7 hours at 37°C, fixed with 3.6%

formaldehyde diluted in PBS, (Grogg-Chemie AG, Stettlen, Switzerland) and stained with DAPI. The percentage area covered by syncytia was calculated as above.

Mice

Ly6e^{tm1a} ES cells were obtained from the EUCOMM consortium[58] and microinjected into C57BL/6J blastocysts by the UTSW Transgenic Technology Center. Chimeric mice with germline transmission were bred to obtain *Ly6e$^{tm1a/+}$* offspring. *Ly6e$^{tm1a/+}$* mice were crossed with FLPe-expressing mice (*B6N.129S4-Gt(ROSA)26Sor$^{tm1(FLP1)Dyn}$/J*, #16226, Jackson Laboratories) to obtain *Ly6e$^{fl/+}$* offspring, which were bred to homozygosity. Conditional *Ly6e$^{fl/fl}$* mice were bred to *Vav1-iCre* transgenic mice (B6.Cg-Commd10$^{Tg(Vav1-icre)A2Kio}$/J, #008610, Jackson Laboratories) to obtain *Ly6e$^{\Delta HSC/+}$* (*Ly6e$^{fl/+}$*; *Vav1-iCre*) offspring. *Ly6e$^{\Delta HSC/+}$* mice were bred to obtain *Ly6e$^{\Delta HSC}$* (*Ly6e$^{fl/fl}$; Vav1-iCre*) offspring, which harbor a deletion of exon 3 and 4 in hematopoietic stem cells (HSC). Experimental animals were obtained by crossing *Ly6e$^{\Delta HSC}$* and *Ly6e$^{fl/fl}$* mice. Genotype was confirmed by PCR of genomic DNA in-house or outsourced to Transnetyx. Ablation of *Ly6e* was confirmed by qPCR in immune cells from spleen, liver, or bone marrow. Animal studies were carried out in specific-pathogen-free barrier facilities managed and maintained by the UTSW Animal Resource Center. All procedures used in this study complied with federal and institutional guidelines enforced by the UTSW Institutional Animal Care and Use Committee (IACUC).

In vivo **infection, viral titers, liver ALT, and liver histology**

Six to twelve-week-old female and male mice were injected intraperitoneally with MHV-A59 diluted in PBS to the indicated titers or PBS for a mock infection control. All infected mice were monitored daily for weight and mortality. Animals that lost more than 20% of their original body weight were euthanized per IACUC guidelines.

Viral titers in liver and spleen were determined from frozen organs after weighing, homogenization, and plaque assay on L929 cells. Alanine aminotransferase (ALT) was measured in fresh, unfrozen serum using VITROS MicroSlide Technology by the UTSW Mouse Metabolic Core. Livers were fixed in 10%

24

neutral buffer formalin, embedded in paraffin, sectioned at 5 µM, and stained with hematoxylin and eosin (H&E). Slides were analyzed by an independent pathologist (UTSW Animal Resource Center) who was blinded to experimental conditions. A numerical score was assigned for degree of inflammation and degree of necrosis for each liver. Inflammatory cell infiltration was scored using the following criteria: 0 = none, 1 = minimal, 2 = mild, 3 = moderate, and 4 = marked. The necrosis score was defined by the percent necrosis. 0 = none, 1 = <2%, 2 = 2-20%, 3 = 21-40%, and 4 = >40%.

Primary cell preparation for flow cytometry

All primary cells were maintained in 10% FBS/10 mM HEPES/1 mM sodium pyruvate/2 mM L-glutamine/1x p-s/RPMI (cRPMI2) unless otherwise indicated.

Primary bone marrow derived macrophages (BMDM) were prepared as described previously[60]. Viable cells were quantified using trypan blue exclusion. BMDM were plated at 2.5×10^4 cells per well in non-treated 24-well tissue culture plates. Cells were infected the next day with 0.1 MOI MHV-A59-GFP and isolated 6 hours post-infection for analysis by flow cytometry.

Splenocytes were prepared by mashing whole spleens against a 70 µM cell strainer. Red blood cells were removed by using RBC lysis buffer (Tonbo Biosciences). Viable cells were quantified using trypan blue exclusion. For *in vitro* infection, splenocytes were plated at 1×10^6 cells per well in non-treated 6-well tissue culture plates. Cells were infected the next day with 1 MOI MHV-A59-GFP and isolated 6 hours post-infection. Infected cells were stained with a fluorescent viability dye (Ghostdye Violet 450, Tonbo Biosciences) and fixed in 1% PFA/PBS. The next day, fixed cells were treated with anti-CD16/CD32 (Tonbo Biosciences) and then stained with antibodies that recognize surface lineage markers and analyzed by flow cytometry.

Livers were perfused by PBS injection into the inferior vena cava and out of the portal vein. Blanched livers were minced with sterile scissors and mashed against a 70 µM cell strainer. Hepatocytes and large debris were pelleted at 60 x *g* for 1 minute, 22°C, with no brake. Intrahepatic immune cell (IHIC) and residual hepatocyte containing supernatants were pelleted at 480 x *g* for 8 minutes, 22°C, with max brake and resuspended in 37.5% Percoll (Sigma-Aldrich)/cRPMI2. Remaining hepatocytes were

25

separated from IHIC by centrifugation at 850 x g for 30 minutes, 22°C, with no brake. Red blood cells were removed from the resulting pellet with RBC lysis buffer (Tonbo Biosciences). Viable cells were quantified using trypan blue exclusion. IHIC and splenocytes (4 x 10^5) from infected or mock-infected mice were stained with a fluorescent viability dye (Ghostdye Violet 450, Tonbo Biosciences), treated with anti-CD16/CD32 (Tonbo Biosciences), stained with antibodies that recognize surface lineage markers, and then fixed in 1% PFA/PBS. Fixed volumes of cell suspensions were analyzed by flow cytometry the next day. Absolute cell counts were determined by multiplying final number of lineage marker-positive cells by dilution factor used to normalize cell counts for antibody staining.

All primary cell samples were resuspended in 3% FBS/PBS and analyzed using a S1000 Flow Cytometer with a A600 96-well plate high throughput extension and compensated using CellCapture software (Stratedigm). Data was analyzed with FlowJo Software (Treestar). The flow gating strategy for liver and spleen immune cells is included in **Extended Data Figure 9**.

Statistical analysis

Differences in data were tested for significance using GraphPad Prism v8.3.1 for Windows (GraphPad). For details regarding the statistical tests applied, please refer to the figure legends. P values < 0.05 were considered significant.

Data availability

The authors declare that the data supporting the findings of this study are available within the article and its Supplementary Information files or are available on request. The RNAseq data discussed in this publication have been deposited in the Gene Expression Omnibus (GEO) database, https://www.ncbi.nlm.nih.gov/geo (GSE146074).

Acknowledgements

Author contributions

S.P., K.B.M., E.M., C.M.R., J.W.S., and V.T. designed the project. S.P., K.B.M., E.M., A.K., D.H., P.V., W.F., N.E., H.S., H.K-W., M.H., H.H.H., M.S., M.W-C., N.W.H. and G.Z. performed experiments. R.D., S.Pö., E.S., and T.G. contributed to the design and implementation of the research.

D.T. performed statistical analysis and analysis of RNA-Seq dataset. S.P., K.B.M., and J.W.S. wrote the manuscript, and all authors contributed to editing.

Competing interest declaration

The authors declare no competing interests.

Supplementary Information is available for this paper.

Materials & Correspondence

Correspondence and requests for materials should be addressed to Volker Thiel, John W. Schoggins, and Charles M. Rice.

Extended Data


```
                                         10        20        30        40        50        60        70
                                         |         |         |         |         |         |         |
Human (H. sapiens, NP_001120685)   MKIFLPVLLAALLGVERASSLMCFSCLNQKSNLYCLKPTICSDQDNYCVTVSASAGIGNLVTFGHSLSKT
Rhesus (M. mulatta, NP_001253648)  MKIFLPVLLAALLGVERASSLMCFSCLNQKSNLYCLKPTICSDQDNYCVTVSTSAGIGNLVTFGHSLSKT
Bat (P. alecto, XP_006913005)      MKVFLPVLLAALLGVEQARSLVCFACTNQNSNLYCLKPTVCSDSDKYCVTVSAAAGIGNVVDLGYSLNKG
Mouse (M. musculus, NP_001157508)  MRVFLPVLLAALLGMEQVHSLMCFSCTDQKNNINCLWPVSCQEKDHYCITLSAAAGFGNV-NLGYTLNKG
Camel (C. dromedarius, XP_006173084) MKVFLPVLLAALLGVERARSLVCFSCTNKNSNWYCLKPTVCSDSDNYCVTISASAGIGNVVDFGYTLNKG
                                     *::*************:*. **:**:* :::.*  ** *. *.:.*:**:*:*:::**:**:  :*::*.*

                                         80        90        100       110       120       130
                                         |         |         |         |         |         |
Human (H. sapiens, NP_001120685)   CSPACPIP-EGVNVGVASMGISCCQSFLCNFSAADGGLRASVTLLGAGLLLSLLPALLRFGP
Rhesus (M. mulatta, NP_001253648)  CSPACPLP-EGINVGVASMGISCCQSFLCNFSAADGGLRASATLLGAGLLLSLLPALLRFGP
Bat (P. alecto, XP_006913005)      CSPVCPAP-PNVNLGVASMGTHCCQSFLCNISAADGGLRASATMLGLGLLLSLLTAVLRLGP
Mouse (M. musculus, NP_001157508)  CSPICPSENVNLNLGVASVNSYCCQSSFCNFSAAGLGLRASIPLLGLGLLLSLLA-LLQLSP
Camel (C. dromedarius, XP_006173084) CSPICPGP--SVNLGVASVGTHCCQSFLCNISAADGGLRASTHVLGLGLLLSLLSALLRLGP
                                     *** **   .:*:****:.  **** :**:***. ***** :** ******* :*::.*
```


Extended Data Figure 1. The antiviral activity of LY6E is evolutionarily conserved and specific to CoVs. a, Duplicate screens depicting HCoV-229E infection (48 hours post-infection) in Huh7 cells expressing ISGs. **b**, Multiple sequence alignment of Ly6e amino acid sequences of different species. **c**, Phylogenetic tree of mammalian LY6E orthologues. **d**, HCoV-229E infection of Huh7.5 cells expressing vector control or human (*H. sapiens*), camel (*C. dromedarius*), bat (*P. alecto*), mouse (*M. musculus*), or rhesus (*M. mulatta*) LY6E orthologues. **e**, Stable LY6E or empty vector expressing

29

Huh7.5 cells infected with MERS-CoV in a limiting dilution assay. **f**, Stable Huh7.5 cells expressing either LY6E or containing empty vector infected with HCoV-229E, HCV, CHIKV, hPIV-3, RSV, SINV, VEEV, WNV, ZIKV, YFV, and DENV. **g**, HCoV-229E-Rluc infection of naïve or stably transduced Huh7 cells expressing empty vector control or LY6/uPAR family members. **h**, HCoV-229E-Rluc infection of Huh7 cells transduced with lentiviruses expressing firefly luciferase (Fluc) control, LY6E WT, LY6E HA or specific block mutants[9]. Data represent average of independent biological replicates, n=3 (**d**), n=3 (**e**), n=3 (**f**), n=3 (**g**), n=3 (**h**). Statistical significance was determined by ordinary one-way ANOVA with Dunnett`s correction for multiple comparison (**d, e, g, h**), 2way ANOVA followed by Sidak's multiple comparisons test (**f**). Error bars: SD. *P* values: **d**, **** p=<0.0001, ** p=0.0030; **e**, * p=0.0118, ** p=0.0013; **f**, **** p=>0.0001, ** p=0.0095, ns= >0.9999 (CHIKV) >0.9999 (PIV) >0.9999 (RSV) >0.9999 (SINV) >0.9999 (VEEV) 0.9679 (WNV) 0.8794 (ZIKV) 0.3172 (YFV) 0.7667 (DENV) (For CHIKV one outlier was removed in the control cells); **g**, **** p=<0.0001, ns p=0.9993 (GPFHBPI) 0.9998 (LY6H) 0.9991 (PSCA) 0.9990 (Ly6G6D) 0.9997 (CD59) >0.9999 (LYPD1) 0.9994 (LYPD2) 0.9997 (GML) 0.9997 (LY6D) 0.9992 (LY6K); **h**, **** p=<0.0001, <0.0001, *** p=0.0005, ns p=0.8472, **** p=<0.0001, *** p=0.0003, **** p=<0.0001, <0.0001, <0.0001, *** p=0.0001, **** p=<0.0001.
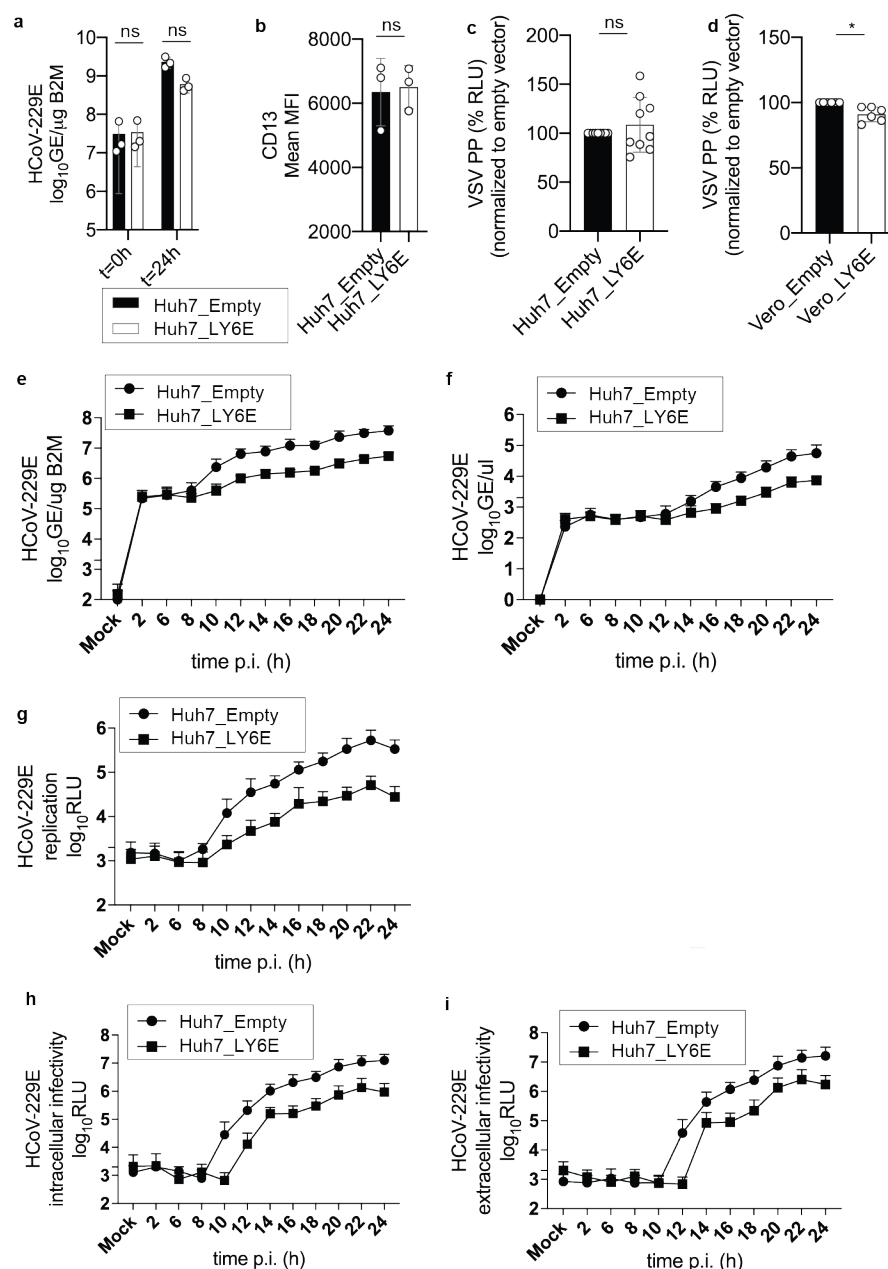
Extended Data Figure 2. LY6E does not affect CoV binding, replication, translation, assembly, or release.

a, Stable LY6E expressing or empty control Huh7 cells were incubated with HCoV-229E and binding analyzed immediately (t=0 h) or after incubation for 24 hours (t=24 h) by RT-qPCR. **b**, Stable LY6E or empty vector expressing Huh7 cells were assessed for surface CD13 expression by flow cytometry. **c,d,** VSV pseudoparticles (PP) harboring VSV-G were inoculated on stable LY6E or empty vector Huh7 cells (**c**) or VeroE6 cells (**d**). **e-i**, Stable LY6E expressing or control Huh7 cells were mock-infected or infected with HCoV-229E-Rluc. Cell lysates were harvested at the indicated time points and intracellular viral RNA was extracted, and viral replication detected via qRT-PCR (**e**). Cell supernatant

31

was harvested and extracellular viral RNA was extracted and viral replication detected via qRT-PCR (**f**). Cell lysates were harvested and intracellular Renilla luciferase activity was detected upon cell lysis (**g**). Cells were subjected to 3 rounds of freeze/thaw cycles. Cell debris was removed and the supernatant titrated on naïve Huh7 cells. Intracellular infectivity was determined (**h**). Supernatant was harvested and titrated on naïve Huh7 cells to determine extracellular infectivity (**i**). Data represent averages of independent biological replicates, n=3 (**a**), n=3 (**b**), n=9 (**c**), n=6 (**d**), n=3 (**e-i**). Statistical significance was determined by 2way ANOVA followed by Sidak's multiple comparisons test (**a**), unpaired student's t-test with Welch's correction (**b, c, d**). Error bars: SD. *P* values: **a**, ns p=0.9448 0.0752; **b**, ns p=0.5188; **c**, ns p=0.3857; **d**, * p=0.0112.
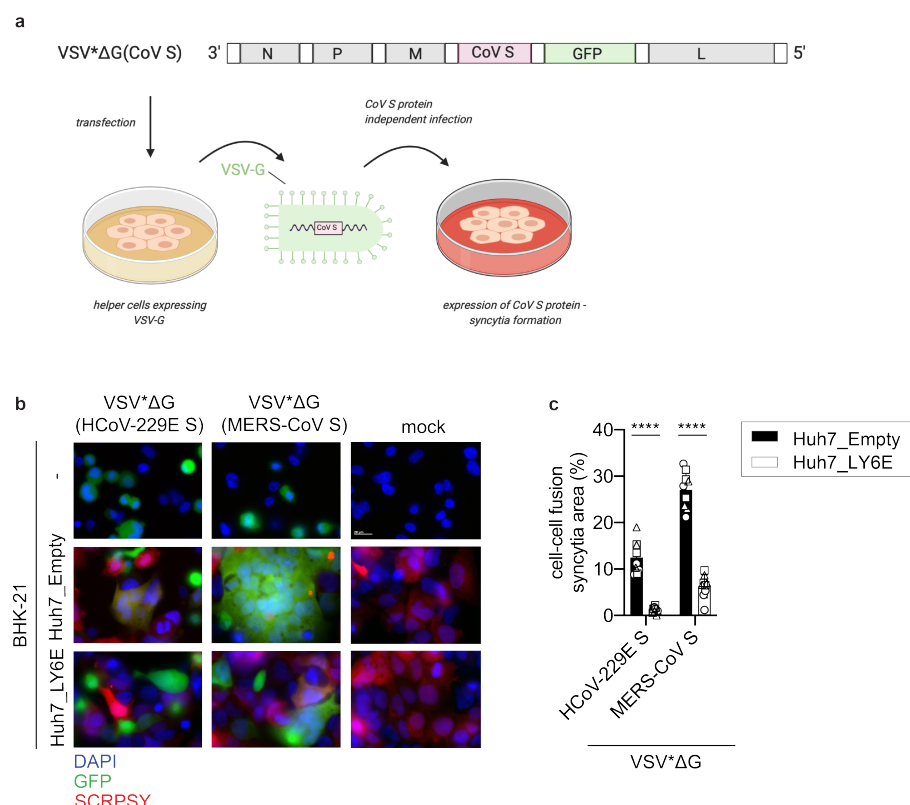
Extended Data Figure 3. Generation of recombinant VSV vector driving CoV S protein expression (VSV*ΔG(CoV)) and heterologous cell-cell fusion assay.

a, Schematic depiction of the generation of recombinant VSV*ΔG(CoV S) expressing both CoV S protein and GFP reporter protein. The respective CoV S genes were inserted into the genomic VSV*ΔG cDNA and recombinant virus was generated in BHK-G43 cells expressing the VSV G protein. The recombinant virus produced in this way harbored the VSV G protein in the envelope allowing CoV S protein-independent infection of cells. Infection of cells with VSV*ΔG(CoV S) led to the expression of CoV S protein and consequent syncytia formation. **b**, Heterologous syncytia formation assay. BHK-21 cells were infected with VSV G protein trans-complemented VSV*ΔG(CoV S) viruses or were mock-infected, followed by co-culture with LY6E or empty control Huh7 cells. Syncytia formation was determined. Blue: DAPI, green: GFP, red: TagRFP encoded in SCRPSY vector. **c**, Quantification of VSV*ΔG(CoV S) induced syncytia depicted as percentage syncytia area. Three independent areas were analyzed per biological replicate (circle, square, triangle). Data represent averages of independent biological replicates, n=3 (**c**). In **b**, scale bar is 20 μM. Statistical significance was determined by 2way

33

ANOVA followed by Sidak's multiple comparisons test (**c**). Error bars: SD. *P* values: **c**, **** p=<0.0001

<0.0001.
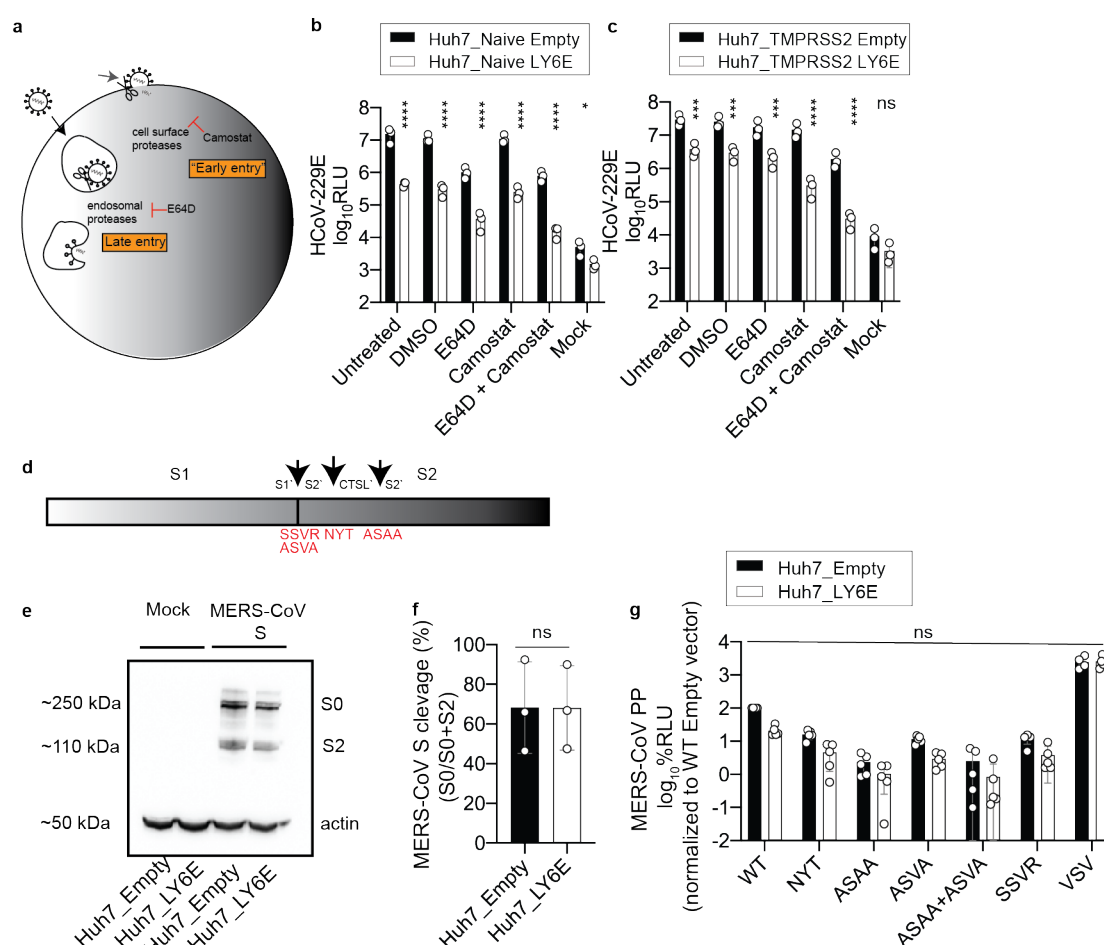
Extended Data Figure 4. The antiviral effect of LY6E is independent of proteolytic cleavage of CoV spike protein.

a, Schematic depiction of cell entry routes of CoVs and intervention by selected compounds. **b-c**, LY6E or empty control-expressing Huh7 cells naïve for (**b**) or ectopically overexpressing TMPRSS2 (**c**) were pre-treated with the indicated compounds before infection with HCoV-229E-Rluc. **d**, Schematic depiction of the CoV spike (S) protein containing the subunits S1 and S2. Arrows indicate the S1/S2' cleavage site, a proposed cleavage site for cathepsin L (CTSL') and the S2' cleavage site. Amino acid exchanges disrupting the respective cleavage sites are depicted in red[17]. **e**, Western blot of S cleavage in LY6E or empty control-expressing Huh7 cells transfected with a plasmid encoding for MERS-CoV S protein (S0= uncleaved, S2= S2 subunit). **f**, MERS CoV S cleavage was analyzed by quantification of S0 and S2 bands. **g**, LY6E or empty control-expressing Huh7 cells inoculated with CoV-pseudoparticles (PP) harboring MERS-CoV S WT or MERS-CoV S proteins containing various

35

cleavage site mutations. Data represent average of independent biological replicates, n=3 (**b**), n=3 (**c**), n=3 (**e**), n=3 (**f**), n=5 (**g**). Statistical significance was determined by 2way ANOVA followed by Sidak's multiple comparisons (**b-c, g**), unpaired student's t-test with Welch's correction (**f**). Error bars: SD. *P* values: **b**, **** p=<0.0001, <0.0001, <0.0001, <0.0001, <0.0001, * p=0.0179; **c**, *** p=0.0007, 0.0005, 0.0006, **** p=<0.0001, <0.0001, ns p=0.1909; f, ns p=0.4968; **g**, ns p=0.9999 (WT) >0.9999 (NYT) >0.9999 (ASAA) >0.9999 (ASVA) >0.9999 (ASAA+ASVA) >0.9999 (SSVR) 0.9867 (VSV).
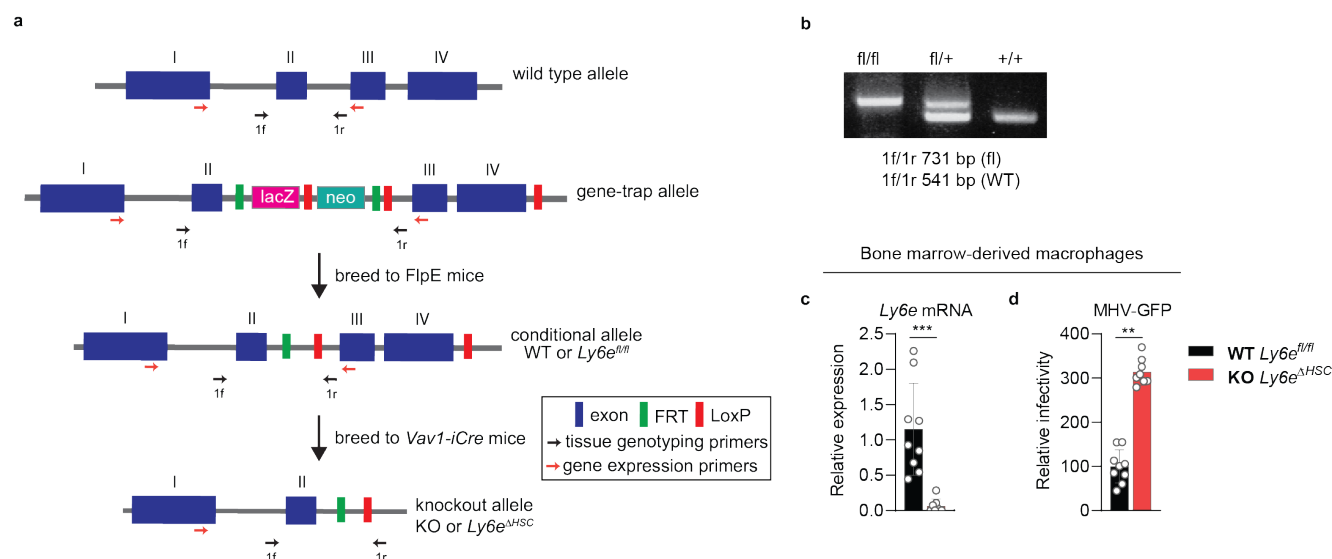
Extended Data Figure 5. Generation of hematopoietic Ly6e conditional knockout mouse.

a, Strategy used to generate $Ly6e^{\Delta HSC}$ mice. Hematopoietic-tissue specific ablation of Ly6e was achieved by crossing $Ly6e^{fl/fl}$ mice with transgenic $Vav1\text{-}iCre$ mice to remove the LoxP-flanked exon III and IV, resulting in a 17 amino acid truncated variant of the 130 amino acid full-length protein. Primers used for tissue genotyping and gene expression are also depicted as arrows. **b,** Gel electrophoresis of tissue genotyping PCR, representing $Ly6e^{fl/fl}$, $Ly6e^{fl/+}$, and $Ly6e^{+/+}$ mice. **c,** $Ly6e$ gene expression in bone marrow-derived macrophages (BMDM). **d,** Infection of BMDM. For **c-d**, n=9 ($Ly6e^{fl/fl}$) or n=8 ($Ly6e^{\Delta HSC}$) mice from three pooled experiments. Data for **c-d** is shown normalized to $Ly6e^{fl/fl}$ values. Statistical significance was determined by using two-tailed unpaired student's t-test with Welch's correction (**c**), two-tailed ratio-paired t-test (**d**). Error bars: SD. P values: **c**, *** p=0.0010; **d**, ** p=0.0021.
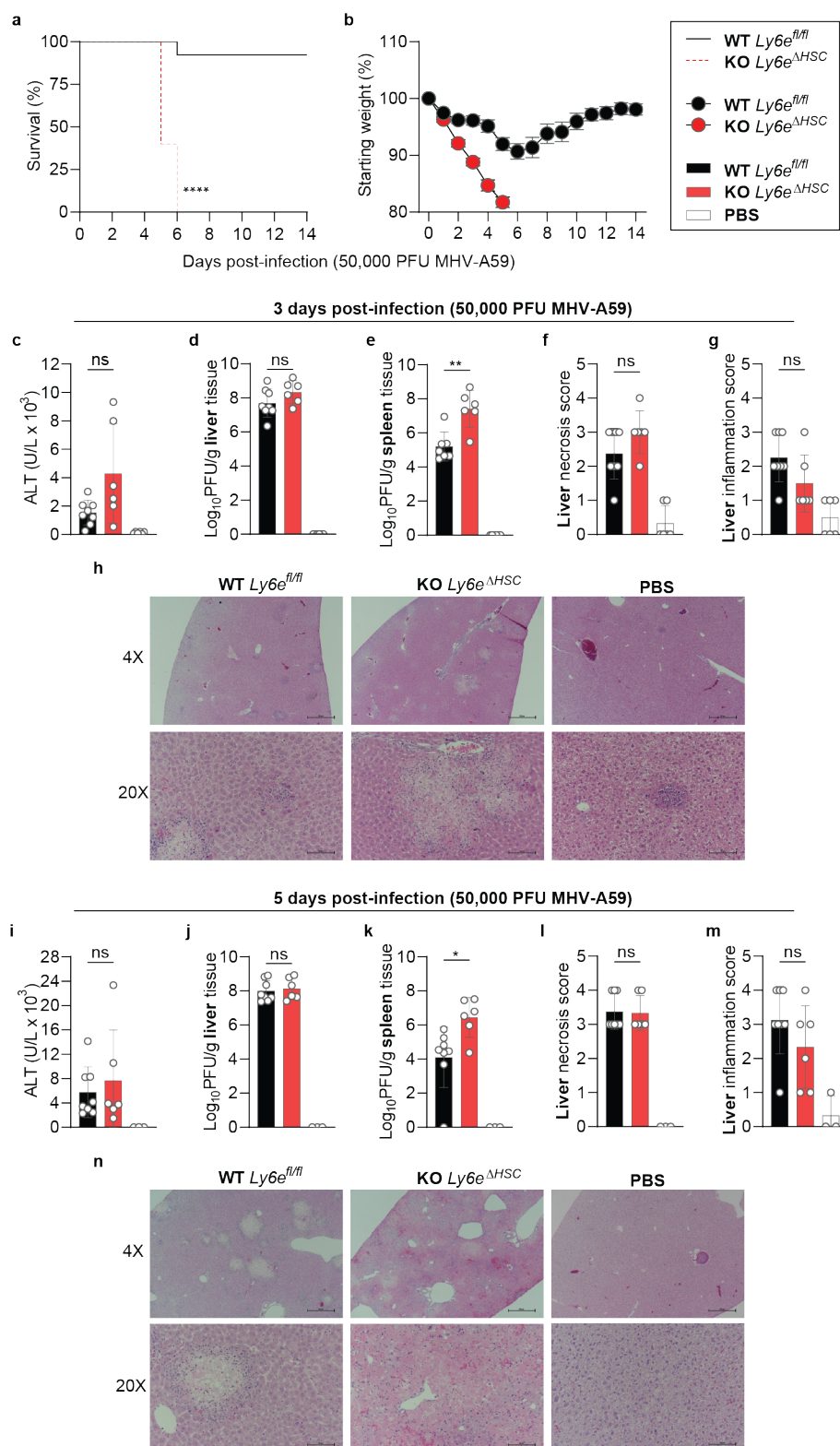
Extended Data Figure 6. *Ly6e^ΔHSC* **mice are susceptible to murine hepatitis virus. a-b**, Male *Ly6e^fl/fl* and *Ly6e^ΔHSC* mice injected with PBS or MHV and monitored for survival (**a**) and weight loss (**b**). **c-n,** Mice were euthanized at 3- (**c-h**) or 5- (**i-n**) days post-infection for determination of serum ALT (**c,i**), viral titers in liver (**d,j**) and spleen (**e,k**), and liver necrosis and inflammation (**f-h**, **l-n**). For **a-b**, n=15 for days 0-6, n=14 for days 6-14, (*Ly6e^fl/fl*), n=10 for days 0-5, n=4 for days 5-6, n=0 for days 6-14 (*Ly6e^ΔHSC*) from three pooled experiments. For **c-g**, n=8 (*Ly6e^fl/fl*,), n=6 (*Ly6e^ΔHSC*), or n=6 (PBS) from

38

two pooled experiments. For **i-m**, n=8 (*Ly6e$^{fl/fl}$*,), n=6 (*Ly6e^{ΔHSC}*), or n=3 (PBS) from two pooled experiments. In **h,n**, scale bars are 500 μM (4x) and 100 μM (20x). Significance for was tested by Mantel-Cox test (**a**), two-tailed unpaired student's t-test with Welch's correction (**c-e**, **i-k**), two-tailed Mann-Whitney U test (**f-g**, **l-m**). Error bars: SEM (**b**), SD (**c-g**, **i-m**). *P* value: **a**, **** p=3.946 x 10^{-6}; **c,** ns p=1144; **d**, ns p=0.1407; **e**, ** p=0.0026; **f**, ns p=0.1708; **g**, ns p=0.0779; **i**, ns p=0.6191; **j**, ns p=0.6842; **k**, * p=0.0119; **l**, ns p>0.9999; **m**, ns p=0.0779.
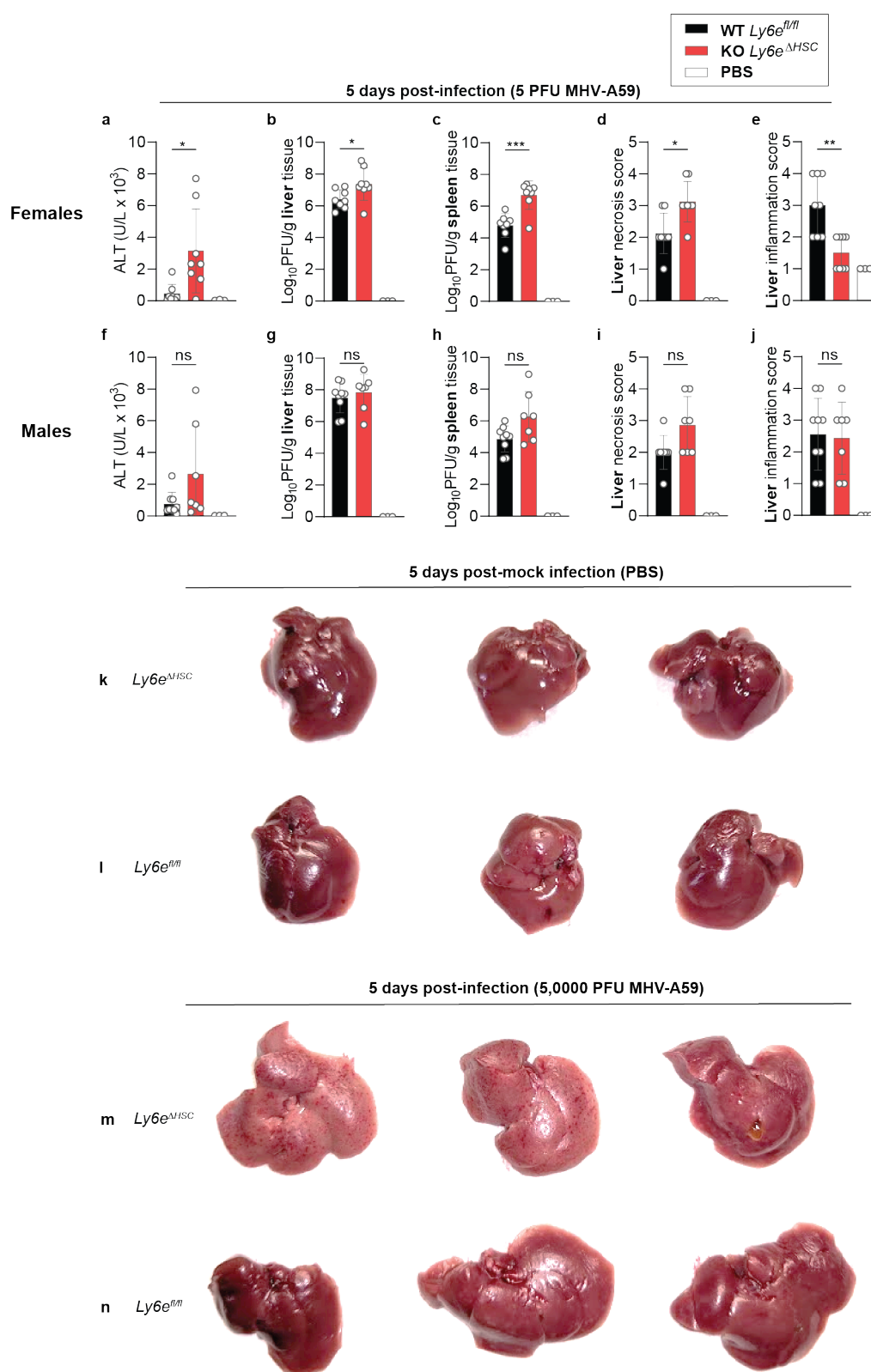
Extended Data Figure 7. *Ly6e$^{\Delta HSC}$* **mice have enhanced sensitivity to murine hepatitis virus.**

a-j, Female (**a-e**) and male (**f-g**) *Ly6e$^{fl/fl}$* and *Ly6e$^{\Delta HSC}$* mice injected with PBS or MHV and assessed for serum ALT (**a,f**), viral titers in liver (**b,g**) and spleen (**c,h**), and liver necrosis and inflammation (**d-e**, **i-j**). **k-n**, Female *Ly6e$^{fl/fl}$* and *Ly6e$^{\Delta HSC}$* mice injected with PBS or MHV and whole livers were imaged. Mock-infected (PBS) *Ly6e$^{\Delta HSC}$* mice (**k**), mock-infected *Ly6e$^{fl/fl}$* mice (**l**), MHV-infected *Ly6e$^{\Delta HSC}$* mice

(**m**), MHV-infected $Ly6e^{fl/fl}$ mice (**n**). For **a-e**, n=8 ($Ly6e^{fl/fl}$,), n=8 ($Ly6e^{\varDelta HSC}$), or n=3 (PBS) from two pooled experiments. For **f-j**, n=9 ($Ly6e^{fl/fl}$,), n=7 ($Ly6e^{\varDelta HSC}$), or n=3 (PBS) two pooled experiments. For **k-n**, n=3. Statistical significance was determined by two-tailed unpaired student's t-test with Welch's correction (**a-c**, **f-h**), two-tailed Mann-Whitney U test (**d-e**, **i-j**). Error bars: SD. *P* value: **a**, * p=0.0234; **b**, * p=0.0428; **c**, *** p=0.0004; **d,** * p=0.0210; **e**, ** p=0.0054; **f**, ns p=0.1544; **g**, ns p=0.5322; **h**, ns p=0.0662; **i**, ns p=0.0592; **j**, ns p=0.9064.
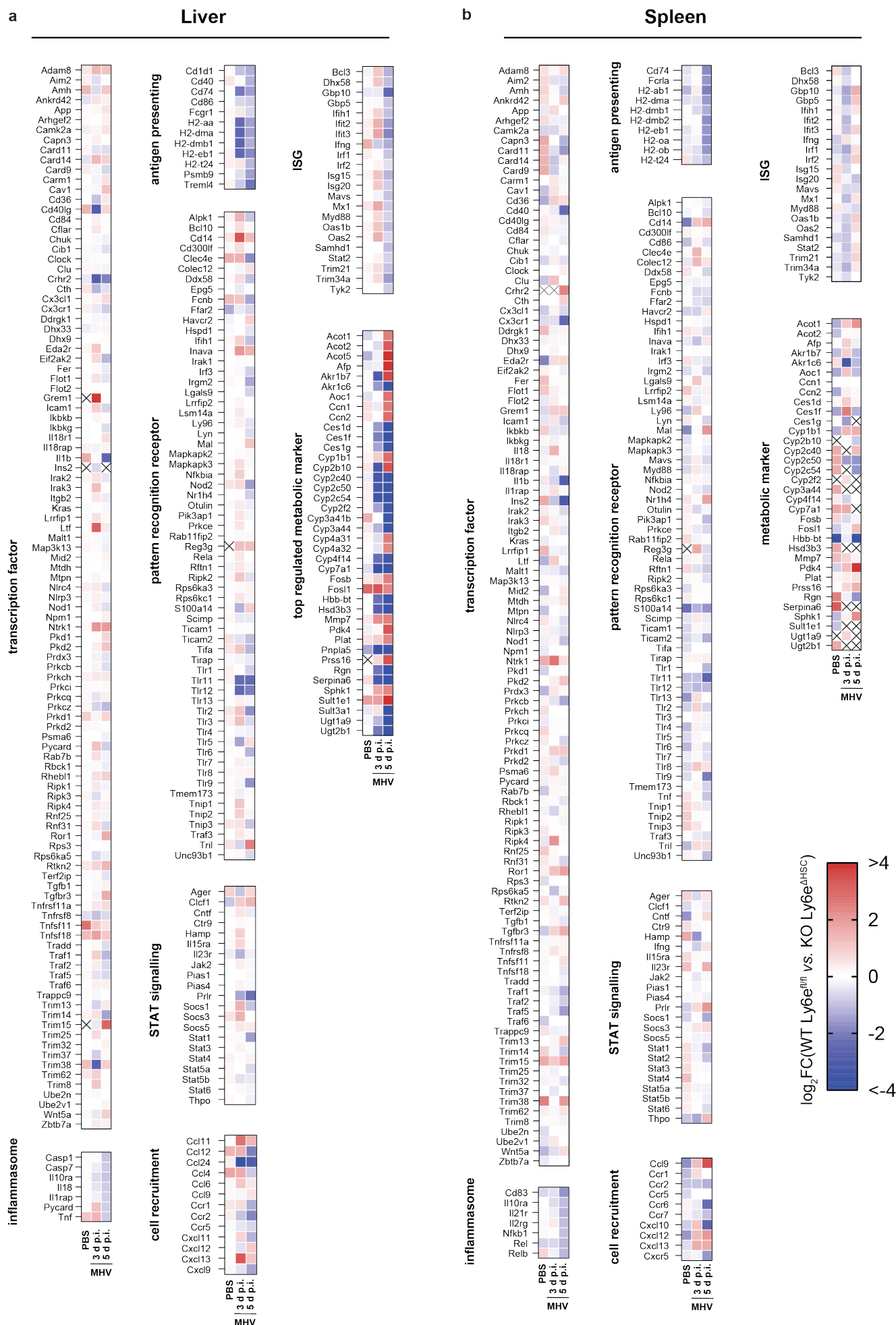
Extended Data Figure 8. Dynamic transcriptional changes in liver and spleen of *Ly6e$^{\Delta HSC}$ vs Ly6e$^{fl/fl}$* mice. Depicted are fold changes in liver and spleen gene expression from *Ly6e$^{\Delta HSC}$* mice compared to *Ly6e$^{fl/fl}$* mice. RPKM values from RNAseq data for liver (**a**) and spleen (**b**) were used to calculate fold changes. Crossed out genes were not detected in either KO or WT mice at respective conditions.

43
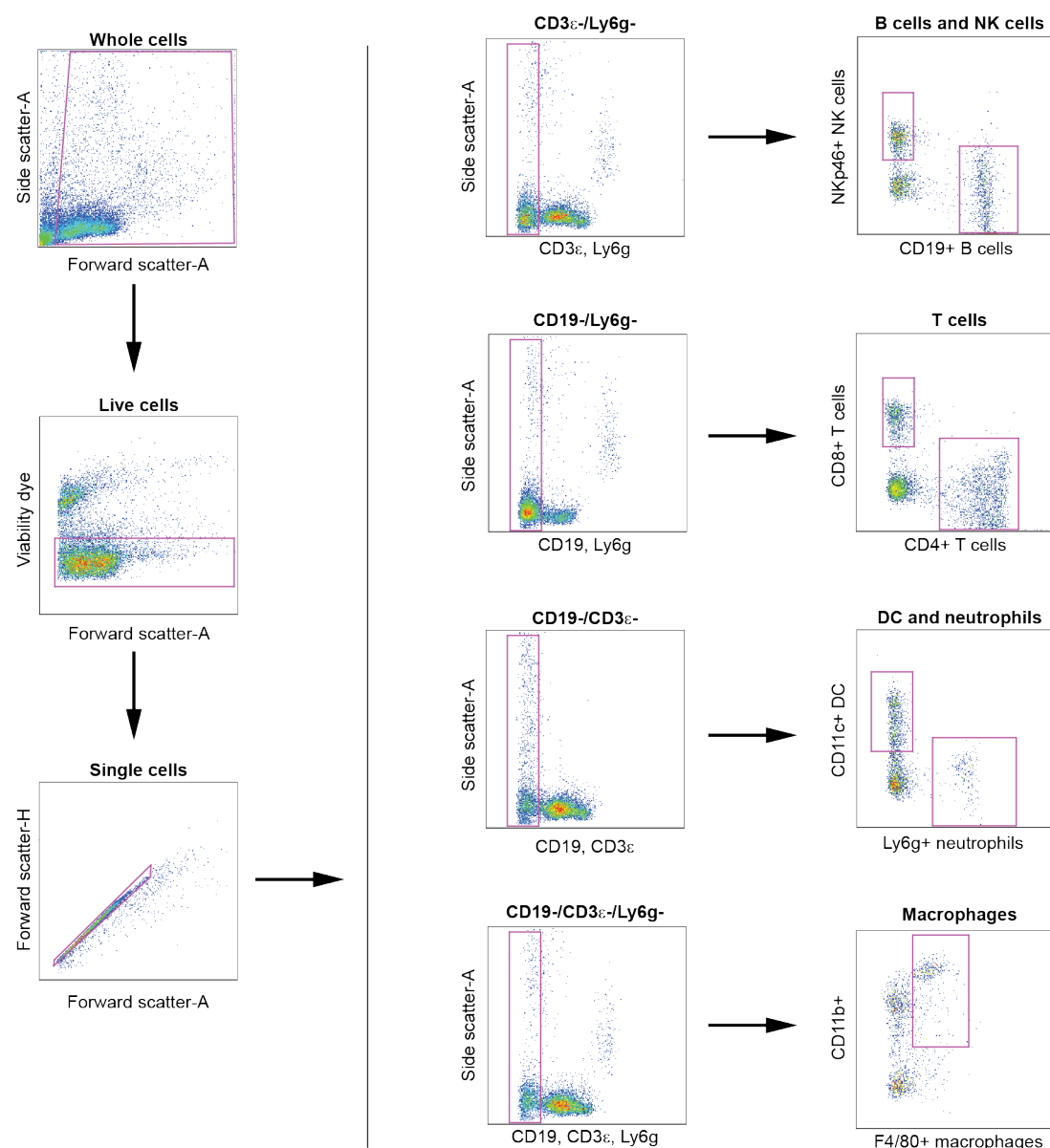
Extended Data Figure 9. Gating strategy for intrahepatic and splenic immune cell identification. Antibody-stained suspensions of isolated intrahepatic immune cells or splenic immune cells were first analyzed by forward scatter/side scatter to remove debris events, then gated for exclusion of a viability dye, and finally for selection of single cell events. A dump-gate strategy was used to identify immune cell populations as indicated in the diagram.
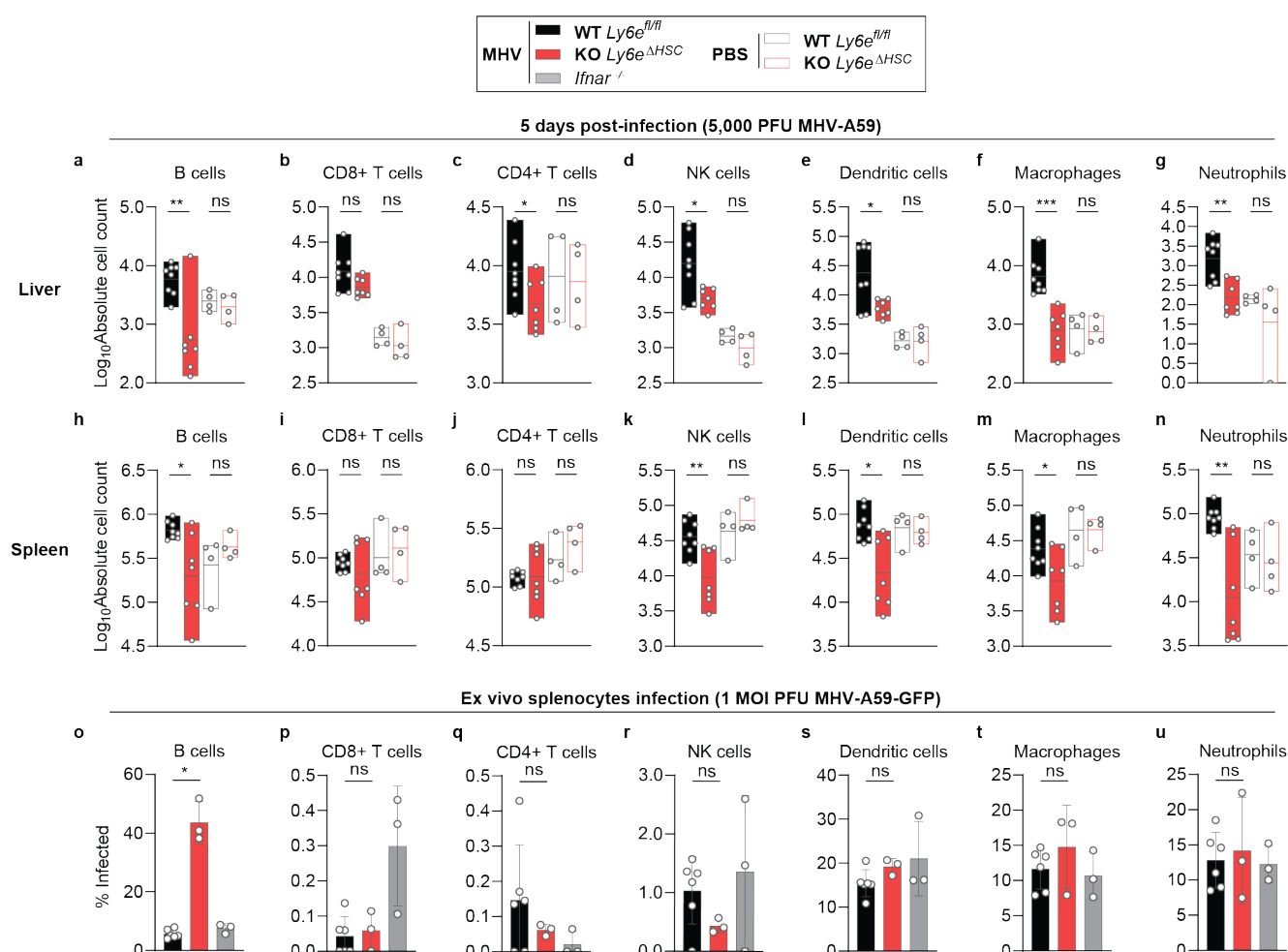
Extended Data Figure 10. Murine hepatitis virus infection significantly alters hepatic and splenic immune cell populations in male *Ly6e^ΔHSC* mice. a-b, Immune cell counts from liver (**a**) and spleen (**b**). **c**, Infection of cultured splenocytes. For **a-b**, n=8 (infected *Ly6e^fl/fl*), n=7 (infected *Ly6e^ΔHSC*), n=4 PBS-injected from two pooled experiments. For **h**, n=6 (*Ly6e^fl/fl*), n=3 (*Ly6e^ΔHSC*), or n=e (*Ifnar^-/-*) mice from two pooled experiments. Statistical significance was determined by two-tailed unpaired student's t-test with Welch's correction (**a-c**). Error bars: SD. *P* values (left-right): **a**, ** p=0.0053, ns p=0.5297, ns p=0.0641, ns p=0.4066, * p=0.0429, ns p=0.8678, * p=0.0163, ns p=0.2261, * p=0.0148, ns p=0.9694, *** p=0.0001, ns p=0.7840, ** p=0.0011, ns p=0.3465; **b**, * p=0.0284, ns p=0.3291, ns p=0.4421, ns p=0.6188, ns p=0.9412, ns p=0.2802, *** p=0.0082, ns p=0.4336, * p=0.0105, ns p=0.6763, * p=0.0419, ns p=0.9712, ** p=0.0046, ns p=0.6857; **c**, * p=0.0105, ns p=0.7080, ns p=0.2470, ns p=0.0503, ns p=0.0568, ns p=0.4637, ns p=0.7915.

Extended Data Table 1. Large scale ISG screen: HCoV-229E in Huh7 at 24 h (page 1 of 2)

Gene	Percent Infected	Z score	Gene	Percent Infected	Z score	Gene	Percent Infected	Z score	Gene	Percent Infected	Z score
CDKN1A	135.7	3.52	CXCL10	107.1	1.01	ANKRD22	101.8	0.55	MTHFD2L	98.0	0.22
SSBP3	129.8	3.00	ALDH1A1	106.9	1.00	THBD	101.8	0.55	NAPA	98.0	0.21
ZNF295	128.2	2.86	TMEM51	106.5	0.96	GLRX	101.7	0.54	TNFAIP6	97.8	0.20
MAFB	127.2	2.78	HES4	106.3	0.94	FAM134B	101.2	0.50	ADM	97.7	0.19
PAK3	126.1	2.68	MX1	106.3	0.94	MSR1	101.1	0.49	CCL8	97.7	0.19
CASP7	121.1	2.24	IL28RA	106.2	0.93	BCL2L14	101.1	0.49	MCL1	97.6	0.18
IFIT2	121.0	2.23	SOCS1	105.9	0.91	DNAPTP6	101.1	0.48	PAD12	97.6	0.18
HK2	120.7	2.20	NMI	105.8	0.90	PRAME	101.0	0.48	CCL19	97.6	0.18
SLC25A28	119.7	2.11	CPT1A	105.7	0.89	CNP	100.9	0.47	BATF2	97.5	0.17
STAT3	118.3	1.99	PARP12	105.7	0.89	USP18	100.9	0.47	CXCL9	97.4	0.17
GCH1	118.1	1.98	HCP5	105.5	0.87	IFI16	100.8	0.46	CREB3L3	97.4	0.16
CTCFL	118.1	1.98	SLC15A3	105.5	0.87	PNRC1	100.7	0.45	GMPR	97.3	0.16
SOCS2	118.0	1.97	ATF3	105.4	0.86	NCF1	100.7	0.45	B4GALT5	97.3	0.15
AHNAK2	117.8	1.95	PPM1K	105.3	0.85	PSMB8	100.6	0.45	TRAFD1	97.2	0.15
CD80	117.1	1.89	CD74	104.9	0.82	LOC400759	100.6	0.45	MAFF	97.2	0.14
EPAS1	117.0	1.88	DTX3L	104.7	0.80	IRF7	100.6	0.44	PDGFRL	97.1	0.14
ARHGAP17	116.4	1.83	DEFB1	104.6	0.80	HSPA6	100.5	0.44	CEACAM1	97.0	0.13
BCL3	116.2	1.81	IGFBP2	104.6	0.79	FLJ39739	100.5	0.44	CHMP5	97.0	0.12
SMAD3	115.3	1.73	MKX	104.2	0.76	MCOLN2	100.4	0.43	C4orf32	96.9	0.12
XAF1	114.9	1.70	FLJ23556	104.2	0.76	CRY1	100.4	0.43	CLEC4A	96.8	0.11
DDX3X	113.3	1.55	UBA7	104.0	0.74	N4BP1	100.3	0.42	PFKFB4	96.7	0.11
IFI44L	112.6	1.49	MICB	104.0	0.74	TRIM5	100.2	0.41	CCL2	96.7	0.11
TREX1	111.9	1.43	RBM43	104.0	0.74	ERLIN1	99.9	0.39	MDA5	96.7	0.10
HESX1	111.8	1.42	TBX3	103.9	0.73	PSCD1	99.9	0.38	TRIM25	96.6	0.10
STAP1	111.4	1.39	TNK2	103.7	0.72	IL6ST	99.7	0.37	RBM25	96.6	0.10
HPSE	111.1	1.36	LGMN	103.7	0.72	EHD4	99.7	0.36	PCTK2	96.5	0.09
FNDC4	110.9	1.34	ARHGEF3	103.6	0.70	EXT1	99.6	0.35	INDO	96.5	0.09
PUS1	110.8	1.33	VEGFC	103.5	0.70	BLZF1	99.5	0.35	RIPK2	96.5	0.08
RSAD2	110.7	1.33	RPL22	103.4	0.69	AQP9	99.5	0.34	LRG1	96.4	0.08
TRIM34	110.7	1.33	ZNF385B	103.4	0.69	ANGPTL1	99.4	0.34	ABLIM3	96.4	0.07
TMEM49	110.6	1.32	SP110	103.4	0.69	IFITM1	99.4	0.34	GZMB	96.2	0.06
MT1G	110.5	1.31	DHX58	103.2	0.67	FCGR1A	99.3	0.33	MAFF	96.2	0.06
TFEC	110.4	1.30	PRKD2	103.1	0.67	DUSP5	99.3	0.33	C9orf19	96.1	0.05
ARNTL	110.2	1.29	SIRPA	103.0	0.66	Empty 1	99.1	0.32	RGS1	96.1	0.05
C15orf48	109.9	1.26	IRF2	103.0	0.65	SIGLEC1	98.9	0.30	PBEF1	96.0	0.04
BAG1	109.8	1.25	SAA1	102.9	0.65	TRIM14	98.9	0.29	GEM	95.9	0.03
NT5C3	109.5	1.23	ADFP	102.9	0.65	P2RY6	98.9	0.29	DCP1A	95.9	0.03
SERPINB9	109.4	1.21	TNFSF10	102.9	0.64	GALNT2	98.8	0.29	S100A8	95.8	0.02
SERPINE1	109.3	1.20	FUT4	102.9	0.64	BUB1	98.8	0.29	TNFAIP3	95.8	0.02
KIAA0040	108.3	1.12	FKBP5	102.5	0.61	VAMP5	98.7	0.28	GBP2	95.7	0.02
HLA-E	108.0	1.09	CCDC92	102.3	0.60	ETV7	98.6	0.27	SAMHD1	95.7	0.02
C10orf10	108.0	1.09	ZNF313	102.3	0.60	MT1L	98.5	0.26	TRIM38	95.7	0.02
SCARB2	107.9	1.09	OPTN	102.3	0.59	CCL5	98.5	0.26	IFI30	95.7	0.02
C9orf91	107.9	1.08	ETV6	102.3	0.59	IDO1	98.4	0.25	C19orf66	95.6	0.01
MS4A4A	107.8	1.08	LINCR	102.3	0.59	Hercb	98.3	0.24	PADI2	95.6	0.00
JUNB	107.8	1.07	CD69	102.0	0.56	LAMP3	98.2	0.24	IFI6	95.3	-0.02
STEAP4	107.6	1.06	CXCL11	102.0	0.56	MTHFD2L	98.2	0.23	NFIL3	95.2	-0.03
COMMD3	107.6	1.05	MT1M	102.0	0.56	TXNIP	98.1	0.22	GBP5	95.2	-0.03
PHF15	107.5	1.05	NOS2A	102.0	0.56	SAMD4A	98.0	0.22	RTP4	95.1	-0.03
LEPR	107.4	1.04	DDIT4	102.0	0.56	ANKFY1	98.0	0.22	PDK1	95.1	-0.04

Extended Data Table 1. Large scale ISG screen: HCoV-229E in Huh7 at 24 h (page 2 of 2)

Gene	Percent Infected	Z score	Gene	Percent Infected	Z score	Gene	Percent Infected	Z score	Gene	Percent Infected	Z score
MT1F	95.1	-0.04	PTMA	91.5	-0.36	NOD2	88.3	-0.63	SAT1	79.8	-1.38
ATP10D	94.8	-0.06	ISG15	91.3	-0.37	C22orf28	88.3	-0.63	BST2	79.6	-1.39
CD38	94.8	-0.06	OAS1	91.3	-0.37	IFI35	88.2	-0.65	UPP2	79.2	-1.43
C5orf27	94.8	-0.07	IL1R	91.2	-0.38	ABTB2	87.9	-0.67	CYP1B1	79.1	-1.44
APOL2	94.8	-0.07	THOC4	91.2	-0.38	ZNF107	87.7	-0.69	ELF1	78.9	-1.45
LGALS9	94.7	-0.07	AIM2	91.2	-0.38	RASGEF1B	87.6	-0.69	NCOA3	78.1	-1.53
CRP	94.7	-0.07	CMAH	91.1	-0.39	IRF9	87.4	-0.71	APOL3	77.9	-1.55
IL17RB	94.7	-0.08	IL15	91.0	-0.40	MAFF	87.3	-0.72	ENPP1	77.8	-1.56
FNDC3B	94.5	-0.09	MOV10	90.9	-0.40	EIF3EIP	87.3	-0.72	GBP3	77.7	-1.56
CX3CL1	94.5	-0.09	IFI44	90.9	-0.41	HEG1	87.2	-0.73	PI4K2B	77.5	-1.58
PABPC4	94.3	-0.10	IFIT1	90.9	-0.41	WARS	87.2	-0.73	MAP3K5	77.0	-1.62
TRIM56	94.3	-0.11	MT1H	90.8	-0.41	PIM3	86.9	-0.76	APOL1	76.9	-1.63
LGALS3	94.1	-0.12	UNC93B1	90.7	-0.42	PMM2	86.8	-0.76	RAB27A	76.4	-1.68
Empty 2	94.0	-0.13	MASTL	90.7	-0.43	MX2	86.8	-0.77	CD274	75.5	-1.76
GBP1	93.9	-0.14	ARG2	90.6	-0.43	FBXO6	86.5	-0.80	IFI27	74.8	-1.82
PMAIP1	93.9	-0.14	PCTK3	90.5	-0.44	ISG20	86.2	-0.81	RNF24	73.4	-1.94
TGFB1	93.8	-0.15	RGL-1	90.4	-0.45	STAT2	86.2	-0.82	UNC84B	73.3	-1.95
TAP1	93.8	-0.15	MARCK	90.4	-0.45	BLVRA	86.1	-0.82	G6PC	73.3	-1.95
FAM70A	93.8	-0.15	CD163	90.3	-0.45	CLEC4D	86.1	-0.83	FAM46A	73.1	-1.96
TNFSF13B	93.8	-0.15	FER1L3	90.3	-0.46	NUP50	85.6	-0.87	supernatantN	73.0	-1.98
TIMP1	93.6	-0.17	GK	90.3	-0.46	MYD88	85.6	-0.87	SPSB1	72.9	-1.98
FAM348	93.4	-0.18	CCL4	90.3	-0.46	GJA4	85.3	-0.90	SLFN12	70.7	-2.17
RBCK1	93.4	-0.19	SLFN5	90.1	-0.47	HLA-C	85.3	-0.90	HERC5	69.0	-2.33
ZBP1	93.3	-0.19	CCNA1	90.1	-0.47	SPTLC2	85.2	-0.91	OAS2	68.5	-2.37
B2M	93.3	-0.20	IRF2	90.1	-0.48	IRF1	85.0	-0.92	NRN1	66.2	-2.57
PML	93.2	-0.20	NDC80	90.1	-0.48	UBE2L6	85.0	-0.93	IFIH2	64.8	-2.69
GTPBP2	93.2	-0.21	CASP1	90.0	-0.48	LMO2	84.9	-0.93	IFITM2	61.2	-3.01
BTN3A3	93.1	-0.22	HERC6	89.8	-0.50	CFB	84.8	-0.94	FAM46C	59.4	-3.17
KIAA0082	93.1	-0.22	CCDC75	89.8	-0.50	STAT1	84.7	-0.95	STARD5	58.7	-3.23
CSDA	92.9	-0.23	C4orf33	89.7	-0.51	SECTM1	84.3	-0.98	SLC1A1	53.5	-3.68
IFNGR1	92.8	-0.24	AMPH	89.7	-0.51	IFITM3	83.6	-1.05	TLR3	44.5	-4.47
RNF19B	92.8	-0.24	ADAMDEC1	89.6	-0.52	RARRES3	83.5	-1.05	SQLE	43.6	-4.55
TAGAP	92.7	-0.25	EPSTI1	89.6	-0.52	IMPA2	83.3	-1.07	LY6E	6.7	-7.78
SLC25A30	92.7	-0.25	CCR1	89.4	-0.53	MAB21L2	83.1	-1.09			
ZC3HAV1	92.7	-0.25	PLSCR1	89.4	-0.53	MAX	83.1	-1.09			
CCND3	92.5	-0.26	GPX2	89.2	-0.55	PFKFB3	83.1	-1.09			
CES1	92.5	-0.26	SLC16A1	89.2	-0.55	KIAA1618	82.9	-1.11			
WHDC1	92.4	-0.27	ODC1	89.2	-0.55	SCO2	82.8	-1.12			
CEBPD	92.4	-0.28	NPAS2	89.2	-0.56	GBP4	82.7	-1.12			
HSH2D	92.3	-0.28	TDRD7	89.1	-0.56	FFAR2	82.7	-1.12			
HLA-F	92.2	-0.29	FAM125B	89.1	-0.57	C6orf150	82.5	-1.14			
ADAR	92.2	-0.29	GCA	89.0	-0.57	FLT1	82.1	-1.18			
AKT3	92.1	-0.30	SERPING1	88.7	-0.59	BIRC3	82.1	-1.18			
CCDC109B	92.1	-0.30	PSMB9	88.7	-0.60	TLR7	82.1	-1.18			
APOL6	92.0	-0.31	AXUD1	88.7	-0.60	TAP2	81.7	-1.21			
RNASE4	91.9	-0.32	LAP3	88.6	-0.60	CLEC2B	81.4	-1.23			
PXK	91.8	-0.32	ULK4	88.6	-0.61	CD9	81.3	-1.25			
Empty 3	91.8	-0.33	OASL	88.6	-0.61	C1S	81.2	-1.26			
HLA-G	91.7	-0.33	RASSF4	88.4	-0.63	IL15RA	81.1	-1.26			
GAK	91.5	-0.35	LIPA	88.3	-0.63	C2orf31	81.1	-1.27			

Extended Data Table 2. Large scale ISG screen: HCoV-229E in Huh7 at 48 h (page 1 of 2)

Gene	Percent Infected	Z score	Gene	Percent Infected	Z score	Gene	Percent Infected	Z score	Gene	Percent Infected	Z score
ZNF107	131.1	3.00	GAK	103.7	0.73	WARS	101.2	0.53	TLR7	98.8	0.33
PAK3	119.7	2.05	C5orf27	103.7	0.73	MT1H	101.2	0.53	IGFBP2	98.7	0.32
PNRC1	118.4	1.95	CLEC4D	103.6	0.72	C15orf48	101.1	0.52	IFIT1	98.7	0.32
LEPR	116.9	1.83	B4GALT5	103.6	0.72	SECTM1	101.1	0.52	COMMD3	98.7	0.32
HSPA6	116.6	1.80	SIGLEC1	103.5	0.72	SSBP3	101.0	0.52	GALNT2	98.7	0.32
CDKN1A	116.4	1.78	SMAD3	103.4	0.71	RPL22	101.0	0.51	TDRD7	98.6	0.31
IL28RA	113.2	1.52	GEM	103.3	0.70	TRIM34	101.0	0.51	NCF1	98.6	0.31
ZBP1	112.6	1.47	OASL	103.3	0.70	LMO2	101.0	0.51	CXCL11	98.6	0.31
KIAA0040	111.5	1.38	MAFF	103.2	0.70	CD69	100.8	0.50	CD274	98.6	0.31
EPAS1	111.3	1.36	SLC16A1	103.1	0.69	MCL1	100.7	0.49	SERPINB9	98.4	0.30
MAFB	109.8	1.24	NAPA	103.1	0.69	FAM125B	100.7	0.48	UBA7	98.3	0.29
RIPK2	109.5	1.21	SP110	103.1	0.69	Empty 1	100.6	0.48	BAG1	98.2	0.28
HES4	109.4	1.20	HCP5	103.0	0.68	PFKFB4	100.5	0.47	AQP9	98.0	0.27
AHNAK2	109.0	1.17	Hercb	103.0	0.67	PRKD2	100.5	0.47	LAP3	98.0	0.27
BATF2	108.8	1.16	RTP4	103.0	0.67	NMI	100.4	0.46	MT1G	97.8	0.25
PLEKHA4	108.7	1.15	AXUD1	102.9	0.67	PML	100.4	0.46	GPX2	97.7	0.24
ALDH1A1	108.4	1.12	ADFP	102.7	0.65	HLA-G	100.4	0.46	DEFB1	97.7	0.24
DDX60	108.2	1.11	SPTLC2	102.7	0.65	ADM	100.3	0.46	PDK1	97.7	0.24
APOL6	108.1	1.10	MICB	102.6	0.65	FUT4	100.2	0.45	IFIT2	97.7	0.24
SLC25A28	108.1	1.10	P2RY6	102.6	0.64	TMEM51	100.1	0.44	C10orf10	97.7	0.24
CTCFL	107.9	1.08	CMAH	102.6	0.64	TLR3	100.1	0.44	LAMP3	97.6	0.23
SCARB2	107.4	1.04	SAA1	102.6	0.64	DCP1A	100.0	0.43	FER1L3	97.6	0.23
TNK2	107.4	1.04	JUNB	102.5	0.64	C6orf150	100.0	0.43	C1S	97.5	0.23
MSR1	107.4	1.04	IL17RB	102.5	0.64	PHF15	99.9	0.42	NDC80	97.5	0.22
TAGAP	107.0	1.01	PMM2	102.4	0.63	PCTK2	99.9	0.42	UNC84B	97.4	0.21
PCTK3	106.6	0.98	SIRPA	102.4	0.63	TBX3	99.8	0.41	APOL3	97.2	0.20
DDX3X	106.3	0.95	BCL3	102.4	0.63	OAS1	99.8	0.41	C4orf32	97.0	0.18
IL6ST	106.2	0.94	TNFSF10	102.4	0.63	CCNA1	99.7	0.41	TNFSF13B	97.0	0.18
PUS1	105.8	0.91	PSMB8	102.3	0.62	PRAME	99.6	0.40	STAT3	96.9	0.18
ZC3HAV1	105.7	0.90	IFI44	102.3	0.62	USP18	99.6	0.40	CCR1	96.9	0.17
HPSE	105.5	0.89	MT1M	102.3	0.62	SAMHD1	99.6	0.40	NOS2A	96.9	0.17
DDIT4	105.5	0.88	ARNTL	102.1	0.61	FLJ39739	99.6	0.40	TFEC	96.9	0.17
LOC400759	105.3	0.87	TAP2	102.0	0.60	GBP2	99.6	0.40	GCA	96.8	0.17
RSAD2	105.2	0.86	SLC15A3	102.0	0.59	CASP7	99.6	0.39	RAB27A	96.8	0.16
NT5C3	105.0	0.84	FAM134B	102.0	0.59	FNDC3B	99.6	0.39	DDX58	96.7	0.16
CX3CL1	104.9	0.83	HK2	102.0	0.59	HLA-C	99.5	0.39	TRIM56	96.7	0.16
VAMP5	104.8	0.83	HLA-F	102.0	0.59	RBM43	99.5	0.39	FAM348	96.6	0.15
IFNGR1	104.8	0.82	CYP1B1	101.9	0.58	HEG1	99.4	0.38	MAX	96.5	0.14
STAT1	104.6	0.81	KIAA1618	101.9	0.58	CCDC109B	99.4	0.38	ADAMDEC1	96.5	0.14
LINCR	104.6	0.81	IFITM1	101.7	0.57	CLEC4A	99.4	0.38	TRIM38	96.5	0.14
MAFF	104.5	0.80	NFIL3	101.7	0.57	CD80	99.3	0.37	EHD4	96.4	0.14
N4BP1	104.5	0.80	CD163	101.6	0.56	TIMP1	99.2	0.36	PBEF1	96.4	0.13
S100A8	104.4	0.80	CRP	101.5	0.56	MS4A4A	99.2	0.36	CXCL10	96.4	0.13
TGFB1	104.3	0.78	IFI44L	101.5	0.55	GBP1	99.1	0.36	MTHFD2L	96.3	0.13
TXNIP	104.2	0.78	MAFF	101.4	0.54	ETV6	99.1	0.35	BIRC3	96.3	0.13
MKX	104.2	0.78	ARHGEF3	101.3	0.54	LRG1	99.0	0.35	PXK	96.2	0.12
ATF3	104.0	0.76	C4orf33	101.3	0.54	HLA-E	98.9	0.34	IL15	96.1	0.11
FKBP5	103.8	0.75	BUB1	101.3	0.54	PSCD1	98.9	0.34	GBP3	96.1	0.10
SERPINE1	103.8	0.75	STAP1	101.3	0.53	EPSTI1	98.9	0.34	ULK4	96.0	0.10
ZNF295	103.8	0.74				RBCK1	98.8	0.33	KIAA0082	96.0	0.10

48

Extended Data Table 2. Large scale ISG screen: HCoV-229E in Huh7 at 48 h (page 2 of 2)

/.	Percent Infected	Z score	Gene	Percent Infected	Z score	Gene	Percent Infected	Z score	Gene	Percent Infected	Z score
RGS1	96.0	0.10	APOL2	93.6	-0.10	DNAPTP6	90.9	-0.32	RBM25	83.8	-0.91
MARCK	96.0	0.10	MT1F	93.5	-0.11	IRF1	90.9	-0.32	EIF2AK2	83.1	-0.97
IFI16	96.0	0.10	ABTB2	93.5	-0.11	SAMD4A	90.8	-0.33	SOCS2	82.3	-1.04
CCL19	95.9	0.09	PMAIP1	93.5	-0.11	TNFAIP3	90.7	-0.34	FNDC4	81.9	-1.07
FLJ11286	95.8	0.08	CD38	93.5	-0.11	TRIM21	90.6	-0.35	ANGPTL1	81.8	-1.08
CEBPD	95.8	0.08	RNASE4	93.5	-0.11	FCGR1A	90.0	-0.40	GBP4	81.7	-1.08
MX2	95.8	0.08	AKT3	93.4	-0.12	RASSF4	89.9	-0.41	B2M	81.7	-1.08
TAP1	95.8	0.08	SERPING1	93.3	-0.12	ETV7	89.8	-0.41	CNP	81.5	-1.10
PARP12	95.7	0.08	SAT1	93.3	-0.13	CSDA	89.8	-0.41	HERC6	81.4	-1.11
UBE2L6	95.7	0.07	supernatantN	93.3	-0.13	FBXO6	89.8	-0.41	LGALS3	81.2	-1.12
DTX3L	95.7	0.07	MX1	93.3	-0.13	VEGFC	89.8	-0.41	IFI27	81.0	-1.14
IFI30	95.7	0.07	ENPP1	93.1	-0.14	G6PC	89.7	-0.42	MAB21L2	80.0	-1.22
EXT1	95.4	0.05	XAF1	93.1	-0.14	BLZF1	89.7	-0.42	PSMB9	78.6	-1.34
CHMP5	95.4	0.05	CEACAM1	93.0	-0.15	CFB	89.4	-0.45	PLSCR1	78.5	-1.34
CXCL9	95.4	0.05	CCDC75	92.9	-0.16	IRF7	89.4	-0.45	LIPA	78.3	-1.37
ABLIM3	95.2	0.03	PABPC4	92.9	-0.16	CCND3	89.1	-0.47	TMEM49	78.1	-1.38
FAM70A	95.2	0.03	C5orf27	92.8	-0.17	RGL-1	89.0	-0.48	IRF2	77.8	-1.40
TRIM25	95.2	0.03	ZNF313	92.8	-0.17	ANKRD22	89.0	-0.48	IL1R	77.5	-1.43
ERLIN1	95.2	0.03	FLJ23556	92.8	-0.17	FFAR2	88.9	-0.48	NPAS2	75.8	-1.57
WHDC1	95.2	0.03	IFITM3	92.6	-0.18	DHX58	88.7	-0.50	IFI6	73.9	-1.72
RARRES3	95.2	0.03	IRF9	92.6	-0.18	IL15RA	88.6	-0.51	RASGEF1B	73.4	-1.76
IRF2	95.1	0.03	NUP50	92.6	-0.18	EIF3EIP	88.5	-0.52	OAS3	73.4	-1.77
ZNF385B	95.1	0.03	CD9	92.5	-0.19	APOL1	88.3	-0.53	HERC5	71.5	-1.93
CCL2	95.1	0.03	CES1	92.5	-0.19	TNFAIP6	88.3	-0.53	SPSB1	71.3	-1.94
MCOLN2	95.0	0.02	STAT2	92.3	-0.20	IDO1	88.2	-0.55	ELF1	71.0	-1.97
CCDC92	95.0	0.02	SLFN12	92.3	-0.21	PADI2	88.1	-0.55	IFITM2	70.7	-1.99
GLRX	94.9	0.01	ARG2	92.3	-0.21	NOD2	88.0	-0.56	NRN1	65.1	-2.45
INDO	94.9	0.01	TRAFD1	92.2	-0.22	LGMN	88.0	-0.56	FAM46A	64.4	-2.52
RNF19B	94.9	0.01	RNF24	92.2	-0.22	ADAR	87.7	-0.59	BST2	62.7	-2.65
CPT1A	94.9	0.01	NCOA3	92.1	-0.22	GK	87.6	-0.60	STARD5	56.9	-3.13
TRIM14	94.9	0.01	PDGFRL	92.0	-0.23	LGALS9	87.4	-0.61	MDA5	56.0	-3.21
GCH1	94.8	0.00	ISG20	92.0	-0.23	STEAP4	87.3	-0.62	IFIH2	51.8	-3.55
C9orf91	94.7	0.00	SOCS1	91.9	-0.24	C9orf19	87.3	-0.62	BCL2L14	48.7	-3.81
GMPR	94.7	-0.01	PIM3	91.8	-0.24	IFI35	87.1	-0.64	OAS2	37.8	-4.71
THOC4	94.7	-0.01	UNC93B1	91.8	-0.25	PI4K2B	86.9	-0.65	SLC1A1	34.1	-5.01
ATP10D	94.6	-0.01	CCL4	91.8	-0.25	GTPBP2	86.7	-0.67	SQLE	17.5	-6.39
BLVRA	94.6	-0.02	MT1L	91.6	-0.26	ANKFY1	86.0	-0.72	LY6E	4.7	-7.45
ISG15	94.4	-0.03	CREB3L3	91.6	-0.26	DYNLT1	85.9	-0.73			
CCL5	94.4	-0.04	C22orf28	91.4	-0.28	CCL8	85.9	-0.73			
TREX1	94.3	-0.04	THBD	91.3	-0.29	TRIM5	85.9	-0.73			
CD74	94.1	-0.06	MASTL	91.3	-0.29	SLFN5	85.4	-0.77			
UPP2	94.1	-0.06	C2orf31	91.3	-0.29	PFKFB3	85.4	-0.78			
AIM2	94.1	-0.06	MYD88	91.3	-0.29	HSH2D	85.2	-0.80			
GJA4	94.0	-0.07	ODC1	91.2	-0.30	GBP5	85.1	-0.80			
DUSP5	94.0	-0.07	CRY1	91.2	-0.30	PTMA	85.0	-0.81			
AMPH	93.9	-0.08	CASP1	91.1	-0.31	GZMB	85.0	-0.81			
PAD12	93.8	-0.08	CLEC2B	91.0	-0.32	FAM46C	84.9	-0.81			
Empty 2	93.8	-0.09	ZNF107	91.0	-0.32	MOV10	84.2	-0.87			
HESX1	93.6	-0.10	OPTN	90.9	-0.32	BTN3A3	84.2	-0.88			
IMPA2	93.6	-0.10	SLC25A30	90.9	-0.32	MAP3K5	83.9	-0.90			

49

Common ISG Aliases

DDX3X - DDX3, VIPERIN - RSAD2, SERPINE1 - PAI 1, IL28RA - CRF2, VEGFC – VRP, SP110 - IFI41, IRF2 - PRIC285, ZNF313 - RNF114, DNAPTP6 - LOC26010, LOC400759 – PSEUDOGENE, PSCD1 - CYTH1, IFITM1 - IFI17, SIGLEC1 – FRAG, CCL5 - SYCA5, CXCL9 – MIG, IFIH1 - MDA5, INDO – IDO, C9orf19 - GLIPR2, PBEF1 – NAMPT, FLJ11286 - C19orf66, TAP1 - ABCB2, IFIT1 - IFI56/ISG56, FER1L3 – MYOF, CCR1 - CMKBR1, TDRD7 - PCTAIRE2BP, SERPING1 - C1NH, ENPP1 - PDNP1, BST2 - THN

Supplementary Information

Methods

Cell lines

Huh7 hepatocarcinoma cells (kind gift from V. Lohnmann), Huh7.5, STAT1$^{-/-}$ fibroblasts (kind gift from J.-L. Casanova), VeroE6 cells and VeroB4 cells (kindly provided by M.Müller/C.Drosten), 293LTV (Cell Biolabs), and A549 cells (ATCC cat# CCL-185) were maintained in Dulbecco's Modified Eagle Medium-GlutaMAX (Gibco) supplemented with, 1 mM sodium pyruvate (Gibco), 10% (v/v) heat-inactivated fetal bovine serum (FBS) (Gibco), 100 μg/ml streptomycin (Gibco), 100 IU/ml penicillin (Gibco) and 1% (w/v) non-essential amino acids (NEAA; Gibco) (cDMEM) BHK-21 (ATCC cat# CCL-10) were maintained in Glasgow's minimal essential medium (MEM) with 5% FBS and 1% tryptose. BHK-G43[57] were cultured in Glasgow's minimal essential medium with 5% FBS. 17Cl1 fibroblasts (gift from S.G. Sawicki) were cultured in MEM supplemented with 10% (v/v) heat inactivated FBS, 100 μg/ml streptomycin and 100 IU/ml penicillin. Cells were either newly purchased or cell line identities (human cells only) verified by a Multiplex human cell line authentication test.

Huh7 cells expressing TMPRSS2 were generated as follows. In order to generate TMPRSS2-encoding retroviral vectors, the open reading frame of human TMPRRS2 was first PCR amplified with primers adding an N-terminal cMYC epitope to the TMPRSS2 coding sequence. The resulting sequence was inserted into a modified version of the pQCXIP plasmid that contains a blasticidin resistance cassette instead of the usual puromycin resistance cassette[17]. Huh7 cells stably expressing human TMPRSS2 were generated by retroviral transduction and selection with the antibiotic blasticidin (50 μg/ml). Following selection, cells were maintained in culture medium (cDMEM) supplemented with 10 μg/ml blasticidin. To generate STAT1$^{-/-}$_CEACAM1 cells, human STAT1$^{-/-}$ fibroblasts were transduced with lentiviruses encoding for the murine CoV receptor CEACAM1 (kind gift from David Wentworth, CDC, Atlanta, USA[59] and subsequently selected with 1 μg/mL puromycin. Stable LY6E expressing cell lines were generated upon lentiviral transduction with SCRPSY LY6E or as control SCRPSY Empty in DMEM containing 4 μg/ml polybrene (Millipore) and 20 mM HEPES buffer solution (Gibco). Cells

were selected using 2-4 µg/mL puromycin and were passaged until all cells in control wells without lentivirus were killed. The puromycin selected cells were further passaged and frozen down for subsequent experiments. The stable cell lines harboring LY6E orthologues have been described before, with the exception of *C. dromedarius*[9]. For this, a gBlock was ordered (XM_031439745.1) and Gateway cloning performed as described previously to generate pENTR and pSCRPSY plasmids[9]. Constructs encoding for Ly6/uPAR family members and LY6E ASM mutants have been described before[9].

To generate clonal LY6E KO cells and CRISPR-resistant LY6E, A549 cells were transduced with lentivirus containing a LY6E-specific sgRNA and Cas9 as described previously[9]. To generate a clonal cell line, the bulk transduced population was plated at single cell dilutions. Candidate clones were screened by Western blot for LY6E expression and Sanger sequencing. Silent mutations in the region targeted by the LY6E-specific sgRNA were introduced into HA-tagged LY6E to generate CRISPR-resistant LY6E (CR LY6E). LY6E KO A549 cells were reconstituted with CR-LY6E by lentiviral transduction and expression confirmed by Western blot.

All cell lines were regularly tested to check they were free of mycoplasma contamination using a commercially available system (PCR Mycoplasma test kit I/RT Variant C, PromKine).

ISG screen.

The ISG screen was performed as described previously with slight modifications[7,8]. Briefly, 5×10^3 Huh7 cells were seeded, transduced with individual lentiviruses, and 48 hours post-transduction infected with HCoV-229E at 33°C. Infection was stopped 24 hours (MOI=0.1) or 48 hours (MOI=0.01) post-infection and plates were immuno-stained as described previously[61] with an anti-HCoV-229E N protein antibody and a AlexaFluor488-conjugated donkey anti-mouse secondary antibody (Extended methods; Antibodies for immunofluorescence and flow cytometry). For high-content high-throughput imaging analysis ImageXpress Micro XLS (Molecular Devices, Sunnyvale, CA) was used as previously described[8]. Hits were normalized to cells expressing the empty vector. Depicted are genes that were

expressed in two independent screens with a transduction efficiency of at least 1 % (cut off). ISGs which were cytotoxic for the cells were excluded from the analysis. Normalized data can be found in **Extended Data Table 1** and **Extended Data Table 2**.

Western blotting.

For SDS-PAGE and Western blot analysis, lysates from cultured cells were prepared using the M-PER Mammalian Protein Extraction Reagent (Thermo) supplemented with protease inhibitors (cOmplete Mini, Roche). Proteins were separated on 10% (w/v) SDS-polyacrylamide gels (Bio-Rad), and electroblotted on nitrocellulose membranes (in a Mini Trans-Blot cell (eBlot L1 GenScript). Membranes were incubated in PBS 0.1% Tween (Merck Millipore) 5% milk (Dietisa, Biosuisse), probed with the respective primary antibodies, followed by incubation with horseradish peroxidase-conjugated secondary antibodies. LY6E was detected using anti-LY6E rabbit monoclonal antibody GEN-93-8-1 (Genentech) at a dilution of 1:5,000 and secondary Peroxidase-AffiniPure Donkey Anti-Rabbit IgG (Jackson Immunoresearch, 711-035-152) at a dilution of 1:10,000. MERS-CoV spike was detected using the monoclonal anti-human 1.6c7 ab (0.12 mg/ml)[62] (kindly provided by B.J. Bosch) at a dilution of 1:1,000 and a secondary Peroxidase-AffiniPure Donkey Anti-Human IgG (Jackson Immunoresearch, 709-035-098) at a dilution of 1:10,000. β-actin was detected using Monoclonal Anti-β-Actin-Peroxidase clone AC-15 (Sigma-Aldrich, A3854) at a dilution of 1:25,000. Proteins were visualized using WesternBright enhanced chemiluminescence horseradish peroxidase substrate (Advansta) and quantified in a Fusion FX7 Spectra (Vilber-Lourmat). Bands were quantified using the respective software (FusionCapt Software Version 18.05).

RNA extraction and RT-qPCR

Viral RNA was extracted from cell lysates (NucleoMag-96RNA kit, Macherey Nagel) or supernatant (NucleoMag-Vet kit, Macherey Nagel) using the KingFisher Flex robot according to the manufacturer's recommendations. The commercially available TaqManTM Fast Virus 1-Step Master Mix (Applied Biosystems) was used for RT-qPCR with 2 μl of RNA input added to 8 μl of prepared mastermix per

sample. Viral RNA was detected using HCoV-229E specific primers normalized to a qRT-PCR standard for HCoV-229E (contains the M gene of HCoV-229E[63]). Intracellular viral RNA was normalized to total RNA (determined via the housekeeping gene Beta-2-Microglobulin (B2M)). Cellular RNA was extracted from cell lysates of Huh7 cells using the Nucleospin RNA kit (Machery Nagel) according to the manufacturer's recommendations, quantified via NanoDrop, and used to generate a standard curve. PCR conditions are available upon request.

Cellular CD13 expression

LY6E expressing or control cells were dissociated (TryPLE Express, Gibco) and enumerated. 3×10^5 cells were stained in duplicate using Zombie Aqua™ Fixable Viability Kit (Biolegend) according to the manufacturer's recommendations. Cells were resuspended in 0.1% FBS/PBS and stained for CD13 expression (See 'Antibodies for immunofluorescence and flow cytometry'). Cells were washed with 0.1% FBS/PBS and resuspend in equal volumes. Cell suspensions were analyzed by flow cytometry using a FACS Canto (BD) and analyzed with FlowJo Software (Treestar).

Binding experiment

Stable LY6E expressing or control Huh7 cells were seeded in a 24-well plate (4×10^4 cells) and mock infected or inoculated with HCoV-229E (MOI=5) in OptiMEM (Gibco) on ice for 1 hour. Cells were washed at least 3x with PBS and harvested immediately (t=0 h) or incubated at 33°C for 24 hours (t=24 h), before cell lysis and extraction of viral RNA as described above. Viral RNA was detected via RT-qPCR normalized to the housekeeping gene B2M as described above.

Time course experiment

8×10^4 cells stable LY6E expressing or control Huh7 cells were seeded in 12-well plates and mock infected or infected with 229E-CoV-Rluc (MOI=0.1) for 2 hours at 33°C in OptiMEM. Cells were washed 3x with PBS and samples harvested at the indicated time points. To determine intracellular replication, cell lysates were collected and viral RNA extracted (NucleoMag-96RNA kit, Macherey

Nagel), followed by RT-qPCR as described before, or cells were lysed using the Renilla Luciferase Assay System kit (Promega) according to the manufacturer's recommendations and Rluc activity determined. To determine extracellular viral replication, viral supernatant was harvested, and viral RNA extracted (NucleoMag-Vet kit, Macherey Nagel), followed by RT-qPCR as described before. To determine intracellular infectivity, cells were subjected to 3 rounds of freeze/thaw cycles, centrifuged to remove debris (4,000 × g for 10 min), and the supernatant titrated on naïve Huh7 cells. To determine extracellular infectivity, supernatant was harvested at the indicated time points and titrated on naïve Huh7 cells. For titration, 1 x 10^4 Huh7 cells were seeded in a 96-well plate and infected with 22 µl of virus containing supernatant and incubated at 33°C. Cells were lysed 24 hours post-infection and infectivity determined using the Renilla Luciferase Assay System kit (Promega) according to the manufacturer's recommendations.

Protease inhibitor treatment

To test various protease inhibitors, 2 x 10^4 naïve or TMPRSS2-expressing, control or LY6E cells were seeded in a 96-well plate. One day post seeding, cells were pre-treated with the following compounds for 1 hour in OptiMEM, at 37°C: DMSO (1:500, Sigma-Aldrich), E64 D (10 µM, Sigma-Aldrich), and/or Camostat (100 µM, Sigma-Aldrich). Cells were mock infected or infected with HCoV-229E-Rluc (MOI 0.1) in the presence of the inhibitors for 2 hours at 33°C. Medium was changed to DMEM and cells incubated for 24 hours at 33°C. Cells were lysed and Rluc activity detected using the Renilla Luciferase Assay System kit (Promega) according to the manufacturer's recommendations.

Spike cleavage assays.

LY6E expressing or control Huh7 (2 x 10^5 cells) were seeded in 6-well cell culture plates. Cells were transfected using Lipofectamine 2000 (Invitrogen) with an expression plasmid encoding for MERS-CoV S (pCAGGS-MERS S). Cell lysates were harvested 48 hours post-transfection and subjected to Western blot analysis as described.

Multiple Sequence alignment and phylogeny

Multiple sequence alignment of LY6E amino acid sequences of different species (NCBI accession numbers provided in the figure) was performed using the EBI web based Clustal Omega tool (doi: 10.1093/nar/gkz268). The phylogenetic tree was built with the "one click" mode for phylogenetic analysis (http://www.phylogeny.fr/) with standard settings (doi: 10.1093/nar/gkn180; doi: 10.1186/1471-2148-10-8).

RNA isolation from primary tissues

Sections of liver and spleen were preserved in RNAlater Stabilization Solution (Thermo Fisher Scientific) and frozen. Thawed samples were transferred to PBS and homogenized. One-eighth of the homogenate was mixed with TRIzol Reagent (Thermo Fisher Scientific). BMDM were directly lysed in TRIzol Reagent and frozen. Total RNA was isolated according to the manufacturer's protocol. Liver and spleen RNA were subject to DNase treatment (TURBO DNA-Free kit, Thermo Fisher Scientific) per the manufacturer's protocol prior to RNA-Seq analysis. BMDM RNA was analyzed by one-step qRT-PCR using QuantiFast SYBR Green RT-PCR Kit (Qiagen) using Applied Biosciences 7500 Fast Real-Time PCR System.

RNA library construction and sequencing

The quantity and quality of the extracted RNA was assessed using a Thermo Fisher Scientific qubit 2.0 fluorometer with the Qubit RNA BR Assay Kit (Thermo Fisher Scientific, Q10211) and an Advanced Analytical Fragment Analyzer System using a Fragment Analyzer RNA Kit (Agilent, DNF-471), respectively. Sequencing libraries were prepared using an Illumina TruSeq Stranded Total RNA Library Prep Gold kit (Illumina, 20020599) in combination with TruSeq RNA UD Indexes (Illumina, 20022371) according to the Illumina guidelines. Sequencing libraries were sequenced paired-end (2 x 50 bp) using an Illumina NovaSeq 6000 S1 Reagent Kit (100 cycles; Illumina, 20012865) on an Illumina NovaSeq 6000 sequencer. The quality control assessments, generation of libraries and sequencing run were all performed at the Next Generation Sequencing Platform, University of Bern, Switzerland.

Data generated from individual samples (>30 million read per sample, single read 50-mers) were mapped separately against the GRCm38 murine reference genome. Gene expression was calculated for individual transcripts as reads per kilobase per million bases mapped (RPKM). All transcriptomic analyses were performed using CLC Genomics Workbench 20 (Qiagen, Aarhaus).

Differentially expressed genes (DEGs) were identified by calculating fold changes in expression, p-values were corrected by taking false discovery rate (FDR) for multiple comparison into account.

Mus Musculus EBI Gene Ontology Annotation Database was used to execute Gene ontology (GO) Enrichment Analyses for biological processes. Gene identifiers for DEGs absolute FC > 5, RPKM > 2) were used as input and identification of significantly enriched GO categories. P-values for specific GO categories were generated after Bonferroni correction for multiple testing. Z-scores, used as indicator for activation of biological processes (positive value) or inactivation (negative value), were calculated based on the expression fold change as follows:

$$z\text{-}score = \frac{(up\text{-}regulated - down\text{-}regulated)}{\sqrt{total\ count}}$$

Antibodies for immunofluorescence and flow cytometry

HCoV-229E infection was detected by staining permeabilized cells for N protein (Anticuerpo Monoclonal, 1E7, Ingenasa) and a secondary donkey anti-mouse AlexaFluor488-conjugated antibody (Jackson Immuno Research). HCoV-OC43 infection was detected by staining permeabilized cells for nucleoprotein (MAB9013, Millipore) and a secondary goat anti-mouse AlexaFluor488-conjugated antibody (Thermo Fisher Scientific). ZIKV infected cells were stained for viral antigen using a monoclonal antibody anti-flavivirus group antigen 4G2 (MAB10216; RRID: AB_827205, EMD Millipore) as primary antibody and AlexaFluor488 (A-11001, RRID: AB_2534069, Thermo Fisher Scientific) as secondary antibody. CD13 was stained anti-human CD13 Antibody, APC conjugated (clone WM15, BioLegend). The following antibodies were used to differentiate immune cell populations: anti-CD3ε-PE (145-2C11, Tonbo Biosciences), anti-CD3ε-FITC (145-2C11, Tonbo

Biosciences), anti-CD11c-PECy7 (N418, Tonbo Biosciences), anti-Ly6G-PE (1A8, Tonbo Biosciences), anti-Ly6G-FITC (1A8, Tonbo Biosciences), anti-Ly6g-PerCPCy5.5 (1A8, Tonbo Biosciences), anti-CD11b-PECy7 (M1/70, Tonbo Biosciences), anti-CD19-PE (6D5, BioLegend), anti-CD19-FITC (1D3, Tonbo Biosciences), anti-CD19-PECy5 (6D5, BioLegend), anti-F4/80-PECy5 (BM8, BioLegend), anti-Nkp46-PECy7 (29A1.4, BioLegend), anti-CD4-PECy5 (GK1.5, Tonbo Biosciences), anti-CD8-PECy7 (53-6.7, Tonbo Biosciences).

Primers and gBlocks

Primer name	Usage	Sequence
Ly6e tissue genotyping forward	Generation of Ly6e^{fl/fl} mice	actcgagttgtcttaatggctacc
Ly6e tissue genotyping reverse	Generation of Ly6e^{fl/fl} mice	cttcagactttggtactggagtgg
Ly6e gene expression forward	qPCR for *Ly6e* expression	atcttcggggcctcttcac
Ly6e gene expression reverse	qPCR for *Ly6e* expression	atgagaagcacatcagggaat
Rpl32 gene expression forward (housekeeping gene)	qPCR for *Rpl32* expression	aagcgaaactggcggaaac
Rpl32 gene expression reverse (housekeeping gene)	qPCR for *Rpl32* expression	taaccgatgttgggcatcag
HCoV-229E M forward	qPCR detection of HCoV-229E	ttccgacgtgctcgaacttt
HCoV-229E M reverse	qPCR detection of HCoV-229E	ccaacacggttgtgacagtga
FAM/BHQ1 probe	qPCR detection of HCoV-229E	FAM-tgggcatggaatcctgaggttaatgc-BHQ1
B2M gene expression forward (housekeeping gene)	qPCR detection of *B2M* expression	tgctcgcgctactctctcttc
B2M gene expression reverse (housekeeping gene)	qPCR detection of *B2M* expression	gtcaacttcaatgtcggatgga
YYE/BHQ1 probe	qPCR detection of B2M	YYE-aggctatccagcgtactccaaagattcaggtt-BHQ1

gBlock Gene Fragment	Usage	Sequence
Gateway Cloning-compatible LY6E sgRNA #4-resistant human LY6E with N-terminal HA epitope tag

CRISPR-resistant LY6E (CR-LY6E) | Reconstitution of LY6E expression in A549 LY6E^{-/-} clonal cell lines | GgggacaagtttgtacaaaaaagcaggcttcaccatgaagatcttcttgccagtgctgctggctgccttctgggtgtggagcgagccagctcgctgatgtgcttctcctgcttgaaccagaagagcaatctgtactgcctgaagccaacaatatgttcagatcaggacaactactgcgtgactgtgtctgctagtgccggcattgggaatctcgtgacatttggccacagcctgagcaagacctgttccccggcctgccccatcccagaaggcgtcaatgttggtgtggcttccatgggcatcagctgctgccagagctttctgtgcaattcTACCCATACGATGTTCCAGATTACGCTagtgcggccgatggcgggctgcgggcaagcgtcaccctgctgggtgccgggctgctgctgagcctgctgccggccctgctgcggtttggcccctgaacccagctttcttgtacaaagtggtcccc |
| Gateway Cloning-compatible *Camelus dromedarius* LY6E | Expression of camel (*C. dromedarius*) LY6E | ggggacaagtttgtacaaaaaagcaggcttcaccatgaaggtcttcctgccggtgctgctggctccctcctgggtgtggagcgagcccgctccctggtgtgcttctcctgcacgaataagaacagcaactggtactgcctgaagcccaccgtctgctccgactccgacaactactgcgtgaccatatctgcatcc |

		gctggcatcgggaacgtggtggactttggctac accctgaacaagggctgctccccgatctgtccc ggcccgagcgtcaatcttggagtggcgtccgt gggcacccactgctgccagagcttcctgtgca acatcagtgcagccgacggcgggctgcgggc cagcacccacgtgctgggcctcgggctcctgc tcagcctgctgtccgccctgctgcggcttggcc cctgaacccagctttcttgtacaaagtggtcccc

References

31   Thiel, V. & Siddell, S. G. Reverse genetics of coronaviruses using vaccinia virus vectors. *Curr Top Microbiol Immunol* **287**, 199-227, doi:10.1007/3-540-26765-4_7 (2005).

32   van den Worm, S. H. *et al.* Reverse genetics of SARS-related coronavirus using vaccinia virus-based recombination. *PLoS One* **7**, e32857, doi:10.1371/journal.pone.0032857 (2012).

33   Bruckova, M., McIntosh, K., Kapikian, A. Z. & Chanock, R. M. The adaptation of two human coronavirus strains (OC38 and OC43) to growth in cell monolayers. *Proc Soc Exp Biol Med* **135**, 431-435, doi:10.3181/00379727-135-35068 (1970).

34   Coley, S. E. *et al.* Recombinant mouse hepatitis virus strain A59 from cloned, full-length cDNA replicates to high titers in vitro and is fully pathogenic in vivo. *J Virol* **79**, 3097-3106, doi:10.1128/JVI.79.5.3097-3106.2005 (2005).

35   Lundin, A. *et al.* Targeting membrane-bound viral RNA synthesis reveals potent inhibition of diverse coronaviruses including the middle East respiratory syndrome virus. *PLoS Pathog* **10**, e1004166, doi:10.1371/journal.ppat.1004166 (2014).

36   Kindler, E. *et al.* Efficient replication of the novel human betacoronavirus EMC on primary human epithelium highlights its zoonotic potential. *mBio* **4**, e00611-00612, doi:10.1128/mBio.00611-12 (2013).

37   Thiel, V. *et al.* Mechanisms and enzymes involved in SARS coronavirus genome expression. *J Gen Virol* **84**, 2305-2315, doi:10.1099/vir.0.19424-0 (2003).

38   Richardson, R. B. *et al.* A CRISPR screen identifies IFI6 as an ER-resident interferon effector that blocks flavivirus replication. *Nat Microbiol* **3**, 1214-1223, doi:10.1038/s41564-018-0244-1 (2018).

39   Berger Rentsch, M. & Zimmer, G. A vesicular stomatitis virus replicon-based bioassay for the rapid and sensitive determination of multi-species type I interferon. *PLoS One* **6**, e25858, doi:10.1371/journal.pone.0025858 (2011).

40   Zhang, L. *et al.* Infection of ciliated cells by human parainfluenza virus type 3 in an in vitro model of human airway epithelium. *J Virol* **79**, 1113-1124, doi:10.1128/JVI.79.2.1113-1124.2005 (2005).

41   Biacchesi, S. *et al.* Recovery of human metapneumovirus from cDNA: optimization of growth in vitro and expression of additional genes. *Virology* **321**, 247-259, doi:10.1016/j.virol.2003.12.020 (2004).

42   Jones, C. T. *et al.* Real-time imaging of hepatitis C virus infection using a fluorescent cell-based reporter system. *Nat Biotechnol* **28**, 167-171, doi:10.1038/nbt.1604 (2010).

43   Schoggins, J. W. *et al.* Dengue reporter viruses reveal viral dynamics in interferon receptor-deficient mice and sensitivity to interferon effectors in vitro. *Proc Natl Acad Sci U S A* **109**, 14610-14615, doi:10.1073/pnas.1212379109 (2012).

44   McGee, C. E. *et al.* Infection, dissemination, and transmission of a West Nile virus green fluorescent protein infectious clone by Culex pipiens quinquefasciatus mosquitoes. *Vector Borne Zoonotic Dis* **10**, 267-274, doi:10.1089/vbz.2009.0067 (2010).

45   Liu, D. *et al.* Fast hepatitis C virus RNA elimination and NS5A redistribution by NS5A inhibitors studied by a multiplex assay approach. *Antimicrob Agents Chemother* **59**, 3482-3492, doi:10.1128/AAC.00223-15 (2015).

46   Suthar, M. S., Shabman, R., Madric, K., Lambeth, C. & Heise, M. T. Identification of adult mouse neurovirulence determinants of the Sindbis virus strain AR86. *J Virol* **79**, 4219-4228, doi:10.1128/JVI.79.7.4219-4228.2005 (2005).

47   Petrakova, O. *et al.* Noncytopathic replication of Venezuelan equine encephalitis virus and eastern equine encephalitis virus replicons in Mammalian cells. *J Virol* **79**, 7597-7608, doi:10.1128/JVI.79.12.7597-7608.2005 (2005).

48   Tsetsarkin, K. *et al.* Infectious clones of Chikungunya virus (La Reunion isolate) for vector competence studies. *Vector Borne Zoonotic Dis* **6**, 325-337, doi:10.1089/vbz.2006.6.325 (2006).

49   Hoffmann, H. H. *et al.* Diverse Viruses Require the Calcium Transporter SPCA1 for Maturation and Spread. *Cell Host Microbe* **22**, 460-470 e465, doi:10.1016/j.chom.2017.09.002 (2017).

50   Torriani, G. *et al.* Identification of Clotrimazole Derivatives as Specific Inhibitors of Arenavirus Fusion. *J Virol* **93**, doi:10.1128/JVI.01744-18 (2019).

51   Gorisek, J. & Marzan, B. [Changes in the blood picture and blood coagulation in calf poisoned by the fern Pteridium aquilinum]. *Wien Tierarztl Monatsschr* **52**, 530-538 (1965).

52   Gierer, S. *et al.* The spike protein of the emerging betacoronavirus EMC uses a novel coronavirus receptor for entry, can be activated by TMPRSS2, and is targeted by neutralizing antibodies. *J Virol* **87**, 5502-5511, doi:10.1128/JVI.00128-13 (2013).

53   Hoffmann, M. *et al.* Differential sensitivity of bat cells to infection by enveloped RNA viruses: coronaviruses, paramyxoviruses, filoviruses, and influenza viruses. *PLoS One* **8**, e72942, doi:10.1371/journal.pone.0072942 (2013).

54   Qing, E., Hantak, M., Perlman, S. & Gallagher, T. Distinct Roles for Sialoside and Protein Receptors in Coronavirus Infection. *mBio* **11**, doi:10.1128/mBio.02764-19 (2020).

55   Hoffmann, M. *et al.* Fusion-active glycoprotein G mediates the cytotoxicity of vesicular stomatitis virus M mutants lacking host shut-off activity. *J Gen Virol* **91**, 2782-2793, doi:10.1099/vir.0.023978-0 (2010).

56   Locher, S., Schweneker, M., Hausmann, J. & Zimmer, G. Immunogenicity of propagation-restricted vesicular stomatitis virus encoding Ebola virus glycoprotein in guinea pigs. *J Gen Virol* **99**, 866-879, doi:10.1099/jgv.0.001085 (2018).

57   Hanika, A. *et al.* Use of influenza C virus glycoprotein HEF for generation of vesicular stomatitis virus pseudotypes. *J Gen Virol* **86**, 1455-1465, doi:10.1099/vir.0.80788-0 (2005).

58   Skarnes, W. C. *et al.* A conditional knockout resource for the genome-wide study of mouse gene function. *Nature* **474**, 337-342, doi:10.1038/nature10163 (2011).

59   Schickli, J. H., Thackray, L. B., Sawicki, S. G. & Holmes, K. V. The N-terminal region of the murine coronavirus spike glycoprotein is associated with the extended host range of viruses

from persistently infected murine cells. *J Virol* **78**, 9073-9083, doi:10.1128/JVI.78.17.9073-9083.2004 (2004).

60   Agac, D., Estrada, L. D., Maples, R., Hooper, L. V. & Farrar, J. D. The beta2-adrenergic receptor controls inflammation by driving rapid IL-10 secretion. *Brain Behav Immun* **74**, 176-185, doi:10.1016/j.bbi.2018.09.004 (2018).

61   Michailidis, E. *et al.* A robust cell culture system supporting the complete life cycle of hepatitis B virus. *Sci Rep* **7**, 16616, doi:10.1038/s41598-017-16882-5 (2017).

62   Widjaja, I. *et al.* Towards a solution to MERS: protective human monoclonal antibodies targeting different domains and functions of the MERS-coronavirus spike glycoprotein. *Emerg Microbes Infect* **8**, 516-530, doi:10.1080/22221751.2019.1597644 (2019).

63   Vijgen, L. *et al.* Development of one-step, real-time, quantitative reverse transcriptase PCR assays for absolute quantitation of human coronaviruses OC43 and 229E. *J Clin Microbiol* **43**, 5452-5456, doi:10.1128/JCM.43.11.5452-5456.2005 (2005).